Max H2 DR

Maximise H2 Enrichment in Direct Reduction Shaft Furnaces

Hybrid demonstration of DR model shafts in demonstration scale

Deliverable D2.3 by WP2. Partners: BFI, RUB, M39

BFI: Yalcin Kaymak, Emanuel Kashi Thienpont, Thomas Piontek, Thorsten Hauck

RUB: Klidi Qyteti, Enric Illana Mahiques, Viktor Scherer

BFI RUHR UNIVERSITÄT BOCHUM RUB

July 2026

This project has received funding from the European Union under grant agreement NUMBER — 101058429 — MaxH2DR

Table of contents

Max H2 DR

List of Figures

List of Tables

1. Introduction

The efficiency and product quality of the direct reduction process are governed by the coupled interaction of gas–solid flow, heat transfer, and reduction kinetics within the shaft furnace. In particular, local variations in solid flow and pressure drop across the packed bed constitute critical parameters, as they significantly influence gas distribution and, consequently, reduction performance.

This deliverable couples experimental results in a demonstration-scale shaft furnace test rig with digital models into the hybrid demonstration approach performed by MaxH2DR.
The demonstrator is operated with a Midrex layout, at cold conditions and with different amount of solid and gas (air) flow. Trials are done using different materials to account for changes in the bulk properties. This will support the extrapolation of results to hot conditions. The local material descent can be optically observed through the transparent front and is recorded and evaluated to calibrate the models.

Two kinds of models are used:

1. A very detailed but extremely computationally expensive DEM approach describing forces and movement of each particle. The DEM model can be coupled with a CFD model to introduce the gas flow.
2. A FEM-model which describes the solid movement with low computational effort in a simplified rheology approach which basically describes the solid flow as a kind of (virtual) fluid.

Several preliminary results are already reported in the deliverables D2.1 and D2.2 (Piontek, Hauck, Qyteti, Mahiques, & Scherer, 2026) (Qyteti, et al., 2024). However, the analyses of the experimental solid descent profiles revealed that the results were significantly affected by artifacts and noise and not reliable and accurate enough, considering their high importance for the unique hybrid demonstration approach of MaxH2DR. Thus, the procedure was completely revised and is reported in this deliverable. These physical results are coupled with the digital results of both models as foreseen by the hybrid demonstration approach.

The resulting hybrid demonstration provides a solid basis for the final scale-up to industrial conditions and for the parameter studies to optimise the DR process.

2. Experimental setups and simulation methods

This chapter is divided into the description of the experimental part and the modelling parts of the hybrid demonstration approach. The fusion of experimental and digital results is described in chapter 3.

2.1 Experimental setup at BFI

A shaft-type test facility (Figure 1) was built to analyze the interaction of particle and gas flow in a Midrex-based direct reduction shaft furnace.

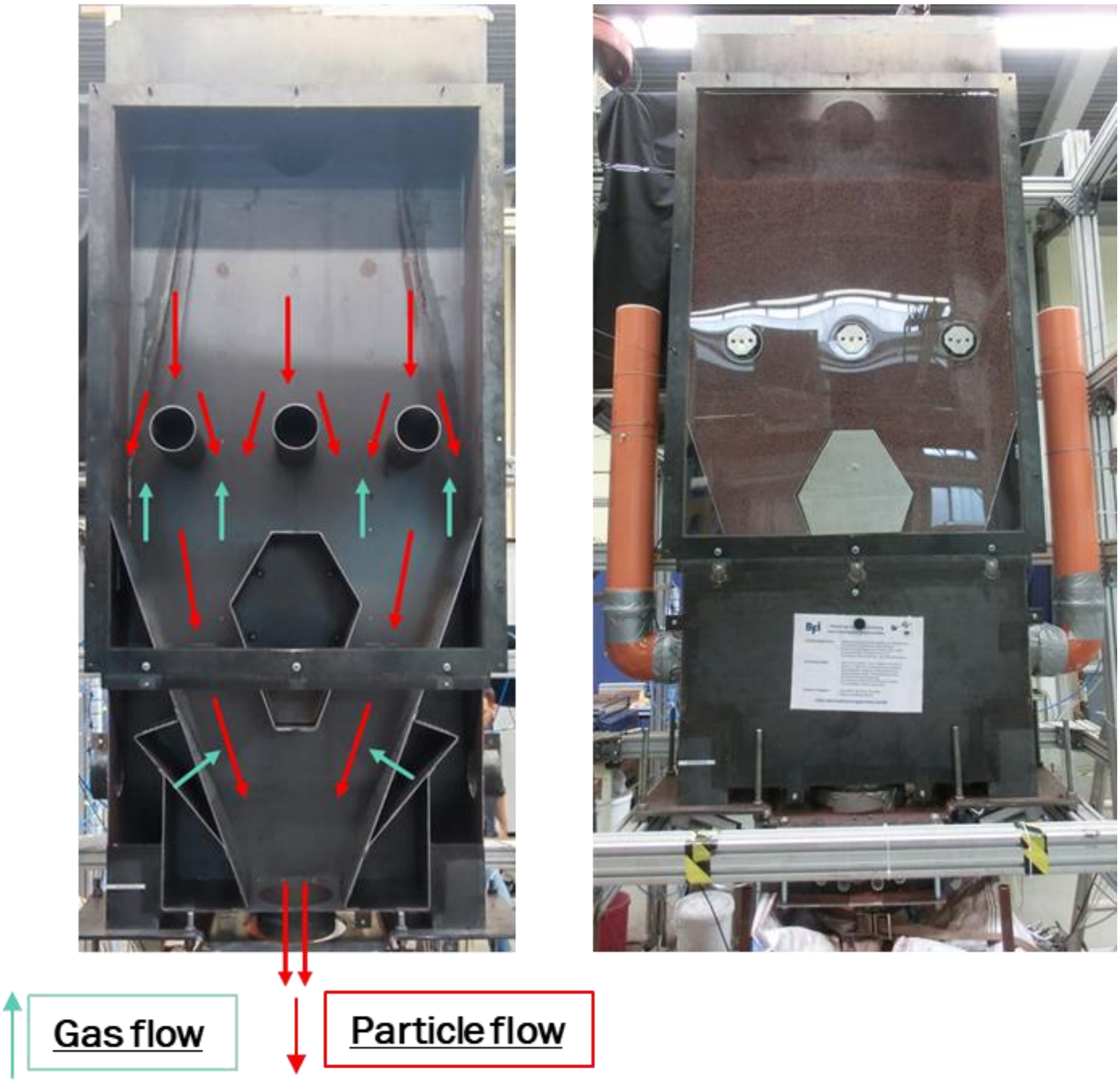

Figure 1: Midrex-based shaft construction to investigate the interaction of gas- and solid flow

The shaft construction in figure 1 is quasi-two-dimensional with a rectangular base. The angle of the side panels can be adjusted for different experimental conditions. The dimensions are 2900x1200x300 mm^3 (Vol. ~1m^3). The setup has two side inlets for the gas (air, see blue arrows in Figure 1). The gas flow is directed upwards to the outlet at the top.

The mass flow of the solids is directed downwards (see red arrows in figure 1) and leaves the test rig through a central outlet at the bottom. This solid outlet is controlled by slide gates at the bottom. The installations inside are exchangeable. In the standard layout, they mimic the installations which are customary for Midrex shaft furnaces.

The pressure drop can be measured for different sections, and the material flow is recorded with a camera through the acrylic front plate and analyzed with MATLAB. Depending on the setting of the slide gates and the ventilator, various operating conditions can be achieved. For the shaft construction, a minimum bulk volume of solid material of 0.8 m^3 is needed. To minimise boundary effects, the particle size should be smaller than 20 mm.

2.2 General Simulation Methods

The numerical simulations were carried out using common input data and modelling assumptions to ensure a consistent comparison with the experimental results. The material properties used in the simulations, such as particle size, density, and shape, were taken from the experimental characterization presented in Section 3.1. The geometry of the simulation model was based on the dimensions of the demonstration shaft, including the internal installations and outlet configuration.

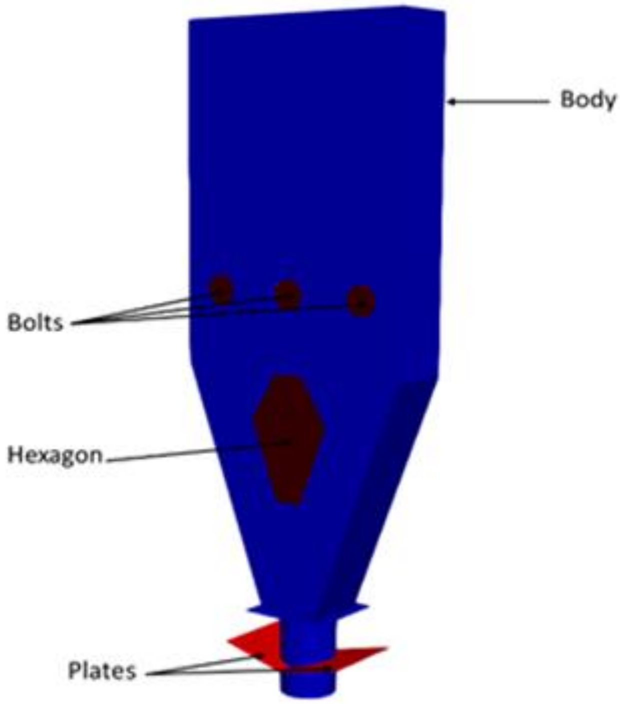

Figure 2: *MIDREX furnace model used for the DEM simulation*

The boundary conditions were chosen to match the experimental setup. The majority of the simulations presented in this deliverable were performed without gas flow, and the same slide opening and material discharge conditions as in the experiments were applied. Suitable mesh sizes and numerical settings were selected to provide stable and accurate solutions while keeping the computational effort at a reasonable level. The mesh was refined in regions where higher flow gradients were expected, particularly around the outlet and internal installations.

Before the final simulations were carried out, the numerical models were calibrated using experimental data. Model parameters were adjusted where necessary to achieve good agreement with the measured particle velocities and overall flow behavior. This calibration provides the basis for the detailed DEM-CFD and FEM simulations presented in the following sections.

2.3 DEM-CFD Method

The DEM-CFD coupling routines available combine the Discrete Element Method (DEM) with Computational Fluid Dynamics (CFD), creating a dual simulation framework. When fluids and bulk solids flow together, both the homogeneous fluid and the discrete solid particles experience intense dynamic interaction. If these processes occur at vastly different timescales, the slower one can be treated as steady state. This allows for calculation of the faster process in a time-dependent manner for a sequence of these static states. For instance, if the blockage of the fluid domain by the solid particles as a "porous medium" that is stationary for a short period is considered, this coupled Stokes flow (for fluids) and Darcy flow (for porous media) problem can be solved using modified incompressible Navier-Stokes equations.

These equations incorporate additional, spatially dependent frictional forces arising from the bulk material [1]. However, it's crucial to choose a small enough time step interval for the Navier-Stokes equations. During this interval, the solid phase is assumed stationary. This ensures that the time evolution of porosity due to fluid interaction is captured accurately. This calculation method also permits complex particle shapes in the simulation, which allow for irregularly shaped polyhedra as model bodies.

The DEM component describes the particle motion of each individual particle, including the forces and contacts between them and any surrounding walls. It essentially solves simplified versions of Newton's laws of motion (for movement) and Euler's equations (for rotation) for every particle, all in real-time. If only contact forces are considered in simplified form, the forms of the equations of motion shown in equations (1) and (2) result. In the case of a simultaneous gas flow, the drag forces formed by the relative velocity must be added to these sums.

$$m_i \frac{d^2 \vec{x}_i}{dt^2} = \sum_{j=1}^{n_{K,i}} \vec{F}_{ij} + m_i \cdot \vec{g} \tag{1}$$

$$\theta_i \frac{d^2 \vec{\varphi}_i}{dt^2} = \sum_{j=1}^{n_{K,i}} \vec{M}_{ij} = \sum_{j=1}^{n_{K,i}} \vec{r}_j \times \vec{F}_{ij} \tag{2}$$

where $d^2\vec{x}_i / dt^2$ is the acceleration, $d^2\vec{\varphi}_i / dt^2$ is the angular acceleration, m_i is the mass and θ_i is the moment of inertia of the particle *i*. $\vec{F}_{ij}$ and $\vec{M}_{ij}$ are the force and moment resulting from contact with particles.

OpenFOAM evaluates the gas–solid momentum exchange using the Ergun drag formulation. Although the pellets are represented as spheres in the DEM domain, a sphericity factor of 0.9 is applied in the Ergun drag formulation to account for the deviation of real pellets from perfect spherical geometry as discussed in Chapter 3.1. The simulations in this study adopt several standard assumptions for DEM–CFD coupling under cold-flow conditions: an isothermal and incompressible gas phase, constant gas properties, no chemical reactions or heat transfer and no-slip wall boundary conditions. These assumptions are consistent with the experimental configuration.

2.4 FEM Method

Compared to DEM-CFD simulation the FEM Method enables a simulation of the DR process with much less computational effort. This enables to run larger parameter analyses to assess process optimisation measures, however, it also needs simplifications with respect to the particle flow. In FEM code for the particle flow has been implemented by a rheology model in the first reporting period (FRP) as described in the first periodic report (MaxH2DR, 2023). Thus, only a short summary is given in the next paragraphs. During the second reporting period (SRP) the rheology model is further calibrated and tuned with the experimental results obtained from Task 2.1. The solid descent velocities observed in the large-scale experiments with the Midrex-shaped setup can be reproduced by the rheology model. Further investigations will be performed to determine the gas flow and solid flow interactions in the FEM code using the Euler-Euler approach (the momentum exchange between gas flow and solid flow).

Summary of Rheology Model: A collection of solid grains can behave macroscopically like a liquid and flow. In the present work, the movement of pellets in the DR reactor vessel is described by Bingham-Papanastasiou model. The yield stress and the apparent viscosity are given by:

$$\tau_y = p \sin \phi \tag{3}$$

$$\mu = \mu_p + \tau_y \frac{1 - \exp(-m_p \dot{\gamma})}{\dot{\gamma}} \tag{4}$$

where τ_y is the yield stress, p pressure, ϕ internal friction angle, $\dot{\gamma}$ shear rate, μ_p and m_p are model parameters.

The wall friction effects can be introduced in the model by using the Navier-Slip boundary condition. This boundary condition enforces no-penetration at the wall, $\mathbf{u} \cdot \mathbf{n}_{wall} = 0$, and adds a tangential stress.

$$K_{nt} = -\frac{\mu}{\beta} u_{slip} \tag{5}$$

where $K_{nt} = K_n - (K_n \cdot n_{wall}) n_{wall}$, $K_n = K n_{wall}$, and K is the viscous stress tensor. β is a slip length, and $u_{slip} = u - (u \cdot n_{wall}) n_{wall}$ is the velocity tangential to the wall.

3. Results

The first sub chapter describes the properties of the sample materials. The second chapter describes experiments and DEM and FEM simulations followed by the fusion of results to provide the hybrid demonstration approach.

3.1 Used bulk materials and their properties

Different particulate materials were employed in the experiments, including monodisperse wooden spheres, industrial direct reduction (DR) pellets, and smaller clay pellets. These materials were selected to represent a broad range of particle sizes, densities, and surface properties. Representative samples of the materials are shown in the following figure.

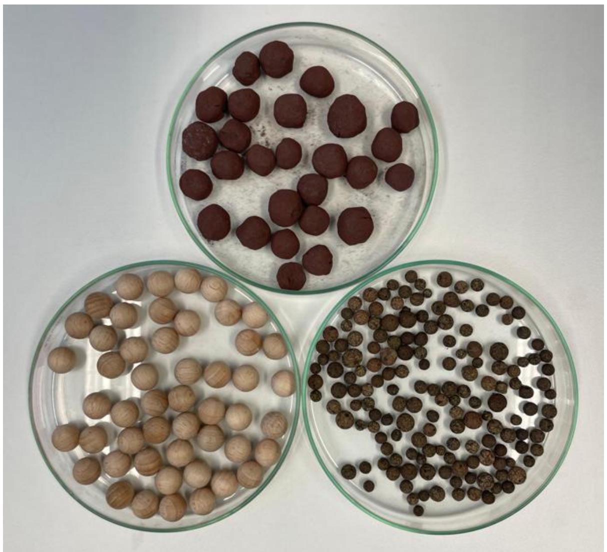

Figure 3: Sample materials used in the experiments: (top) industrial DR-Pellets; (bottom left) monodisperse wooden spheres; (bottom right) clay pellets.

The distributions of particle size and particle shape were determined using continuous image evaluation methods. The measurements are repeated after a certain number of tests to check for particle wear effects. The particle size distributions have a significant influence on the bulk porosity as well as on the pressure drop in the bulk, which again is linked to solid flow via the force transmission between gas and bulk flow.

Measurements are made with the so-called "Camsizer", shown in Figure 4, which is based on the principle of static image analysis. This device from Retsch Technology can analyze and evaluate particles from 20 µm - 30 mm.

Figure 4: Camsizer for the determination of particle size and shape distribution

For the analysis of the particles a representative sample must be taken first. The particles are stored in big bags. From these, samples were taken and mixed from different positions of the bulk material, i.e. from above, the respective sides, or by moving the bulk material also below the surface. In the measuring device "Camsizer" shapes and sizes are determined, and the sample quantity is 500-1000 g in each case. The respective distribution curves and sphericity are then calculated from this.

The size and shape distribution of DR-Pellets were measured before the experiments and after 30 experiments to quantify the change of geometry The particle size distribution received can be seen in Figure 7.

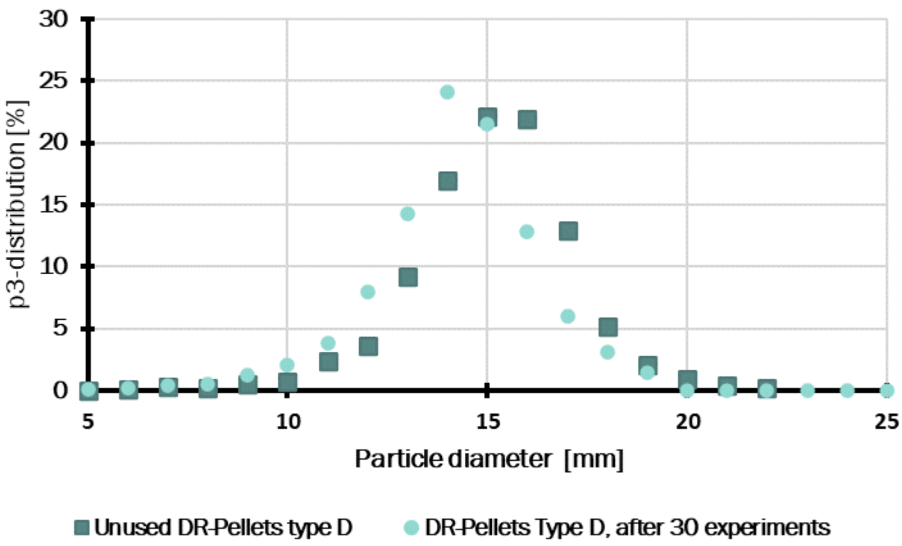

Figure 5: Particle size distribution of the DR-Pellets (Type D)

The distribution of the DR-Pellets during usage shifted slightly to smaller sizes as expected due to deterioration. The sphericity of the particles which represent the similarity to a sphere increased during the experiments.

The clay pellets have the smallest diameter of all the test materials (see following figure) and are mainly used to vary the physical bulk material properties and improve the relation of the particle diameter to the demonstrator size, thus, the deterioration is neglected.

The mean diameter of the DR-Pellets is 14.3 mm of the clay pellets 5.9 mm and of the wooden spheres 12.0 mm. The characteristics of the particles are summarized in Table 1. The bulk porosity was determined from the mass of material filled into the shaft and the corresponding volume of the filled section of the shaft furnace.

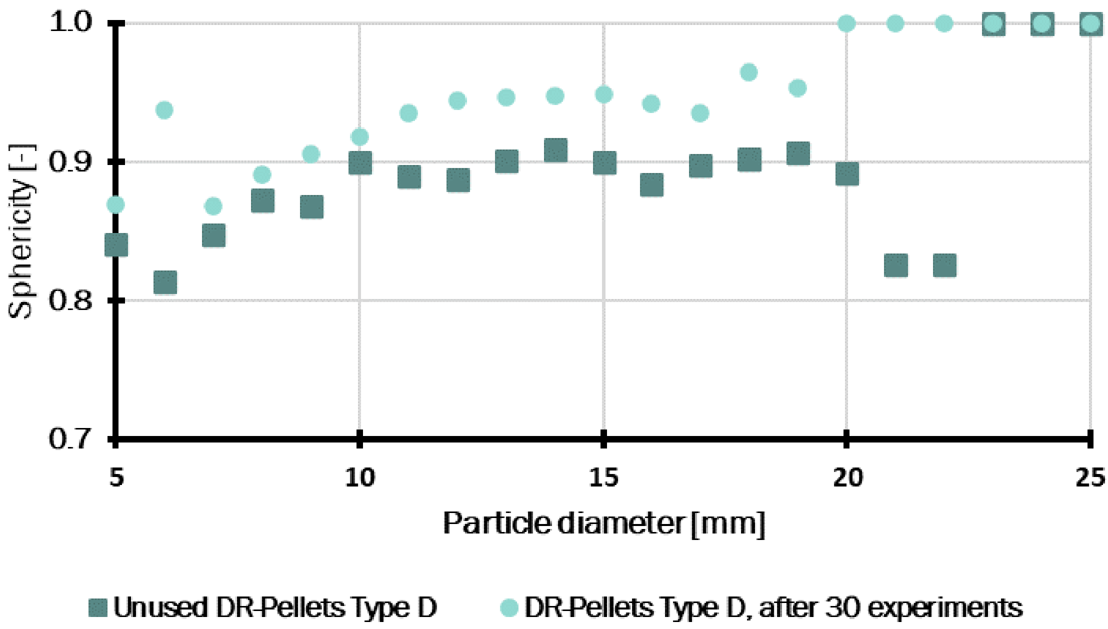

Figure 6: Sphericity of the DR-Pellets (Type D)

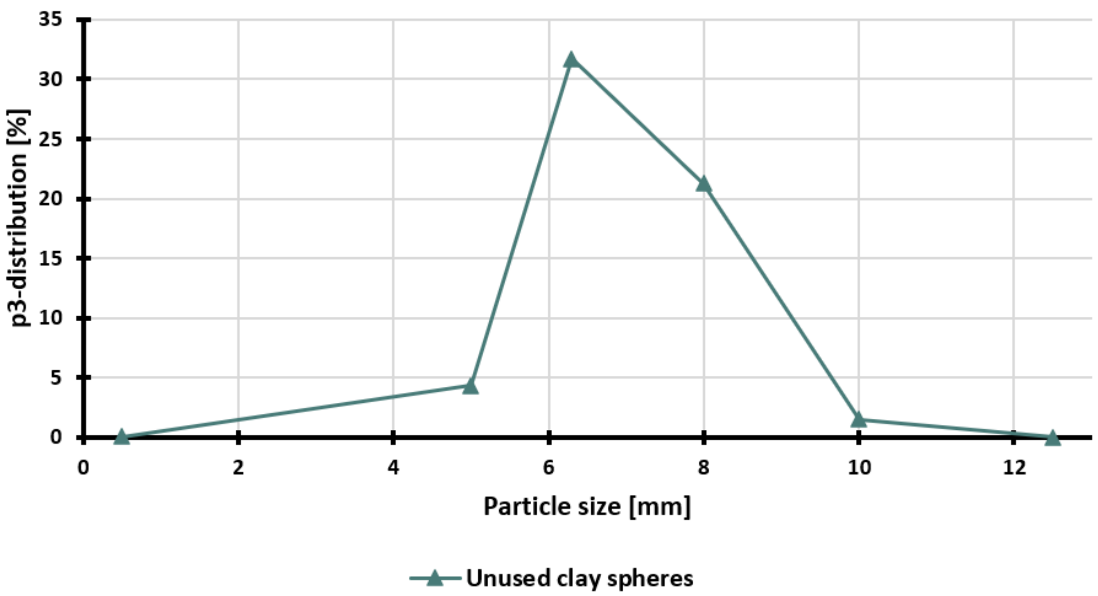

Figure 7: Particle size distribution of clay pellets

Table 1: Overview of the particle and bulk characteristics of the sample material

Material	***D50 diameter [mm]***	***Sphericity [-]***	***Bulk density [kg/m^3]***	***Bulk Porosity [-]***
Wooden spheres	12.0	1	424	0.435
Clay pellets	5.9	0.994	312	0.365
Unused DR-Pellets	14.3	0.936	2181	0.421

3.2 Experiments in the BFI shaft demonstrator

Particle movement

The demonstration trials the particle movement in the shaft construction on different particles, i.e. DR-Pellets, Clay pellets and Wooden spheres, were conducted under different conditions (cf. Section 2.1). The particle movements were recorded by a camera taking videos of the transparent front of the demonstrator. In a next step, a particle image velocimetry (PIV) algorithm was applied to extract the local decent rates from the videos.

Initial results on particle velocity profiles were already presented in Deliverable 2.1 (Piontek, Hauck, Qyteti, Mahiques, & Scherer, 2026). However, the analyses revealed that the PIV results were significantly affected by artifacts and noise. As a result, mean velocities of 10.6 mm/s were obtained for DR-Pellets, compared with 8.9 mm/s derived from ultrasonic distance measurements, while Clay pellets yielded a mean velocity of 7.2 mm/s compared with 4.4 mm/s from the ultrasonic measurements. The impact of these issues was even more pronounced in the determination of local descent profiles. Since the accurate determination of local descent profiles represents a major added value of the MaxH2DR hybrid demonstration approach, these findings highlighted the need for a substantial revision of the video evaluation procedure.

The preprocessing of each recorded video file starts with a digital post processing of each recorded video frame. In the first step the RGB-frame is loaded and transformed into a Black and White (BW) picture as the later applied velocity conversion works only on BW frames. Figure 8 and Figure 8 (A+B) show pictures with DR pellet (Figure 8) and DR and wooden pellet (Figure 8) filling of the demonstrator. With respect to the optical recognition of particles, wooden pellets are by far the easiest material wooden pellets provide obviously a much easier task due to clear contrasts while DR pellets and clays are poorly distinguishable due to their heterogeneous surface structure. Furthermore, pellet trials suffer from pollution and scratches on the front window with dust and clay trials from the small particle sizes, as depicted in Figure 9.

To improve the primary data quality, a new digital enhancement of the BW images was developed. To remove disturbances outside of the shaft construction, the BW figure was overlayed with a mask to exclude almost all unnecessary regions in the image. Furthermore, the contrast was enhanced and background noise removed, cf. Figure 8 C. After the digital postprocessing of the video frames, the “Flow Farneback[1]” algorithm is applied to the BW frames. The Flow Farneback algorithm estimates the velocity of pixels from two subsequent frames by two-frame motion estimation using a polynomial expansion transform approach[2]. The results of this algorithm are x- and y- velocity components derived between every pair of BW frames and are stored in matrices.

---

[1] https://de.mathworks.com/help/vision/ref/opticalflowfarneback.html, 28.07.2026

[2] Farnebäck, Gunnar, Two-Frame Motion Estimation Based on Polynomial Expansion, Image analysis, 2749, 2003, pp. 363-370, doi: 10.1007/3-540-45103-X_50

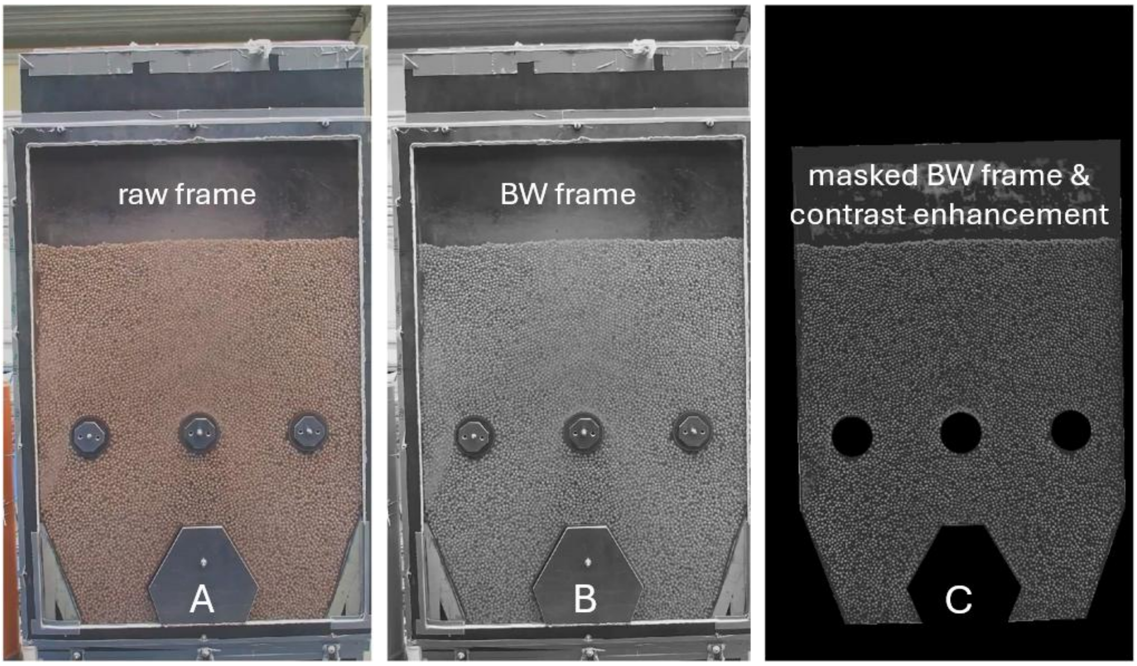

Figure 8: Initial Preprocessing of video frames for Wood, A: raw frame, B: transformation to BW frame, C: masked BW frame including contrast enhancement for better particle visualization.

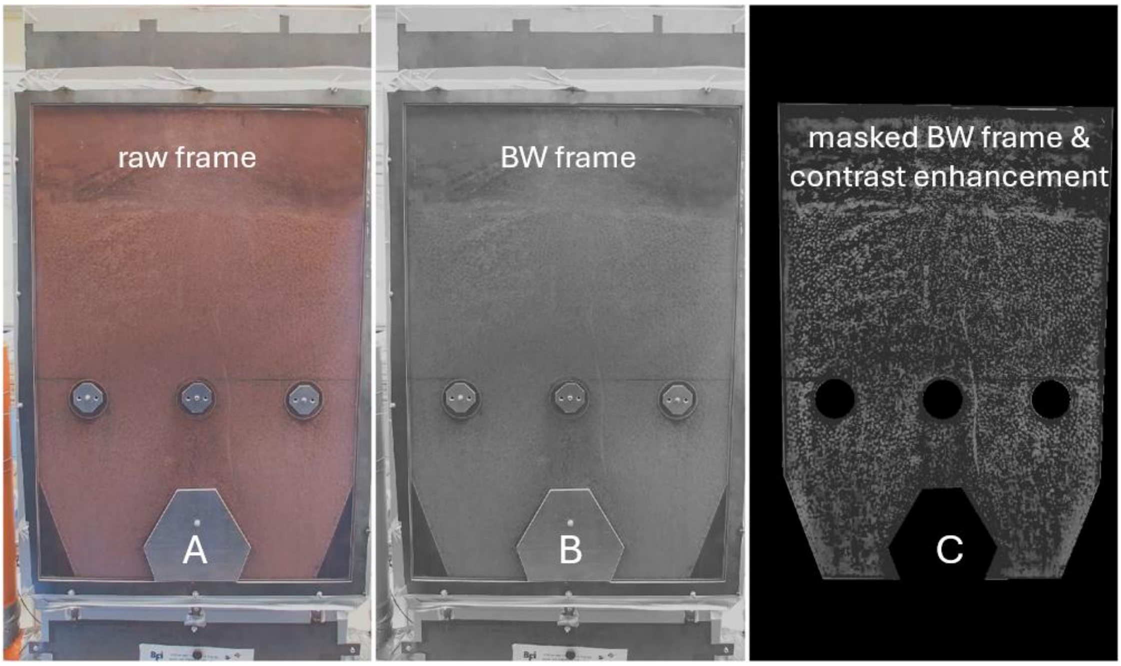

Figure 9: Initial Preprocessing of video frames for DR Pellets, A: raw frame, B: transformation to BW frame, C: masked BW frame including contrast enhancement for better particle visualization.

Figure 10 shows the resulting velocities as arrows by three examples of resulting velocity matrices. The left and middle (Figure 10 A+B) show implausible velocity matrices with large areas without recognized velocities. During the preprocessing, it turned out that the chosen video format as well as the frame rate can have a strong impact on the quality of results. Lossless (but very large) video formats can improve the particle velocity extraction, thus, for the new processing procedure all pixel movements are stored, even when nearly no movement is recognized by the human eye.

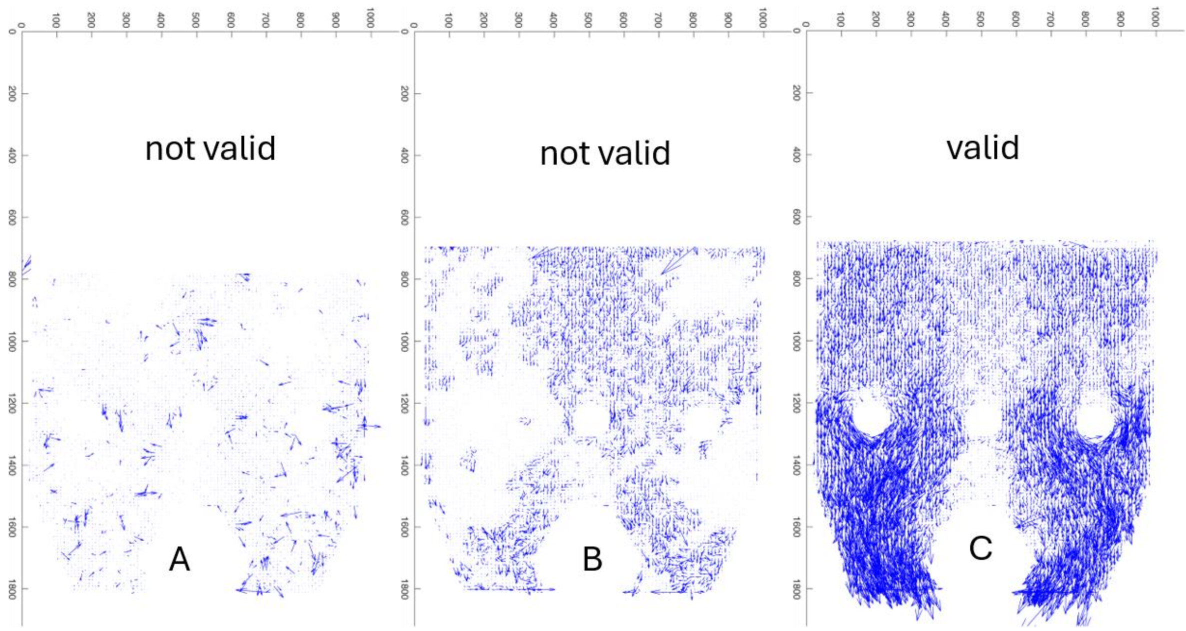

Figure 10: Example of implausible and plausible velocity matrices.

Unrealistic velocity matrices were removed by filtering velocity matrices with mean velocities ≤ 0 mm/s. This step removed a desirable amount of (implausible) velocity matrices and significantly speeds up the further calculation steps. However, local outliers are not affected by this step (cf. Figure 10 C in the lower part), thus, the remaining velocity matrices are filtered locally by removing all velocities outside a range of e.g. <-20 and >40 mm/s. This range can be adopted by considering the expected mean decent velocity of each particle type or experimental setup by the measured average decent velocity. These steps significantly improve the resulting local decent profiles, however, still a considerable amount of fluctuations remains, attributable to vibrations, external disturbances, or variations of real particle motion behaviour which is characteristic for particle motion in general[3].

The conversion of velocities from pixels/s to mm/s is carried out by measuring a known distance in one frame, e.g. the distance between the christmas tree and the centre of the cylindrical insert, and converting it with the pixel distance at a frame duration of 1/30s. This conversion is done once per trial and material (particle type), and is assumed to be constant for one trial and video. As shown in Figure 11, the depiction of the shaft construction in the video frames is tilted by the camera perspective, which influences the local conversion. Thus, the evaluation levels are distorted (cf. red lines), resulting in inaccurate level width over the shaft construction height. To overcome these deviations, the width was rescaled at known distances (cf. Figure 12). This procedure significantly improves the local accuracy of the determined decent velocities and enables a clear assignment to the exact position in the shaft construction. Thus, the influence of the installations on the local particle flow can be determined with much higher accuracy.

In the next step, a 3D median filter (window in three directions) is applied on the remaining pre-processed velocity matrices over a window of +/- 30 velocity matrices (+/- 1 second), 2x particle height (decent or y-direction of the particles) and 1x particle width (x-direction). The final resulting

[3] Dietmar Schulze, Pulver und Schüttgüter, 4. Edition, 2019, Springer Vieweg, pp. 53

filtered velocity matrices are used to extract the final velocity profiles, the previously defined levels over the shaft construction height, as visualised in Figure 11.

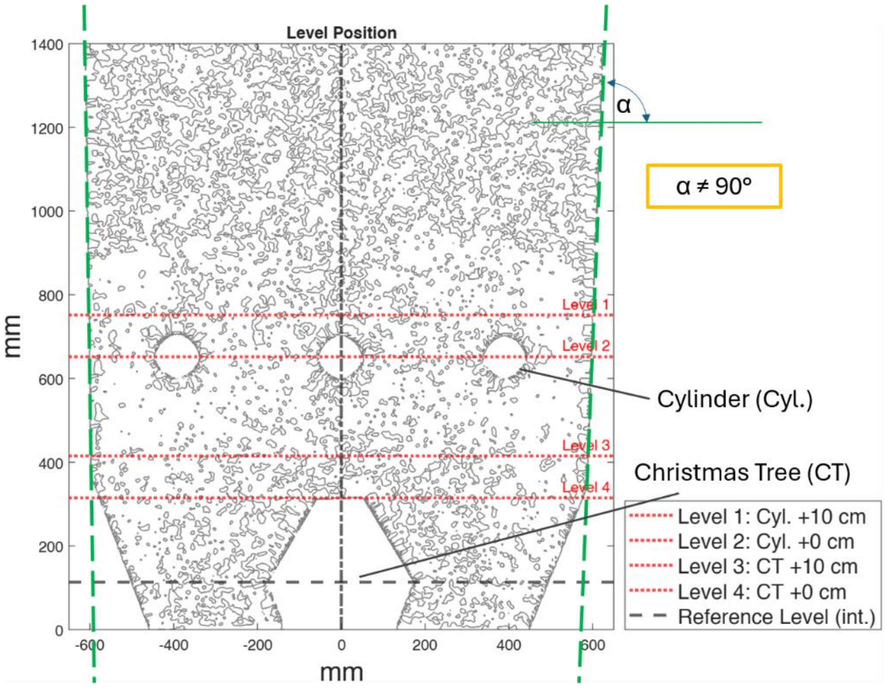

Figure 11: Schematic figure to depict different evaluation levels over shaft construction height.

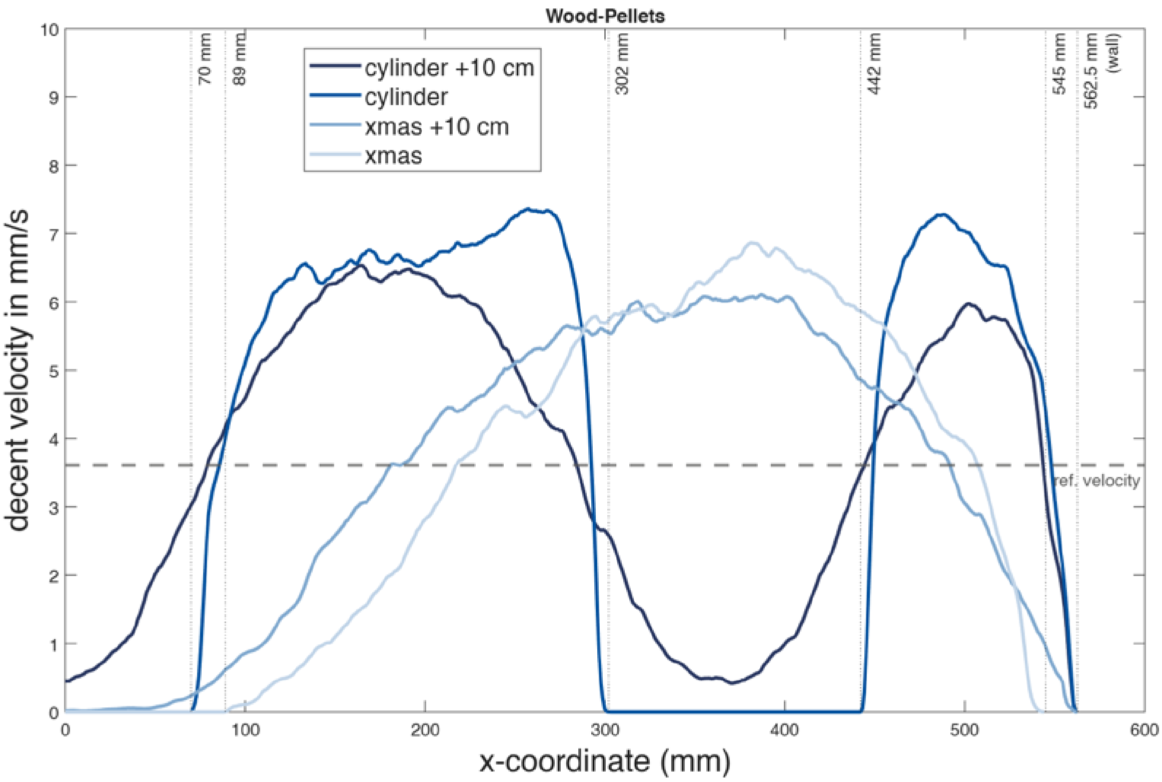

Figure 12: Median decent velocity for wood spheres on different evaluation levels (depicted for half shaft construction width), mean decent vel. 3.8 mm/s (level 1 and 3), ref. vel. 3.61 mm/s.

The values on each level over the complete shaft construction width are used to generate a folded version of the velocity development. It is folded at the symmetry axis at x = 0 mm by calculating the median of both, folded and unfolded velocity values. The symmetrical velocity profiles representing one half of the shaft constructions are summarized for all evaluation levels exemplary shown in Figure 12. This figure shows the decent profiles from center to wall for wood spheres (mean particle size: 12 mm) for four defined reference heights (refer also to Figure 11): From 10cm above the cylindrical installations (very dark blue), via medium height of the cylindrical installations (dark blue), via 10cm above the “christmas tree” (lighter blue) down to the top of the “christmas tree” (very light blue). In Figure 13, each evaluation level is depicted separately, including the information of the variance, to get an impression of how strongly the velocity values fluctuate over the shaft construction width. The degree of the filtering (removing implausible velocity matrices) was optimised checking the consistency of volume flows at different heights.

To visualise fluctuations with time respectively the consistency of the decent velocities during the trial, Figure 14 shows the time dependency of the gained velocity curves on evaluation level 2 (Cyl. + 0 cm) over the whole shaft construction width by addition of a time axis. Not all velocity matrices were depicted in Figure 14, but 131 evenly distributed random samples over the complete duration of approx. 89 seconds of the trial (video length). Figure 14 indicates that the velocity maximum on each side (near to the wall) changes from time to time but e.g. increases on one side and decreases on the other side simultaneously, ensuring an almost constant mean decent velocity. In this type of presentation (cf. Figure 14), the temporal development cannot be easily recognised. For that reason, all considered velocity matrices (reduced to one mean velocity on level 1 (Cyl. + 10 cm)) were depicted at real time in Figure 15, including the total mean velocity (3.51 mm/s) and the measured reference decent velocity (3.61 mm/s).

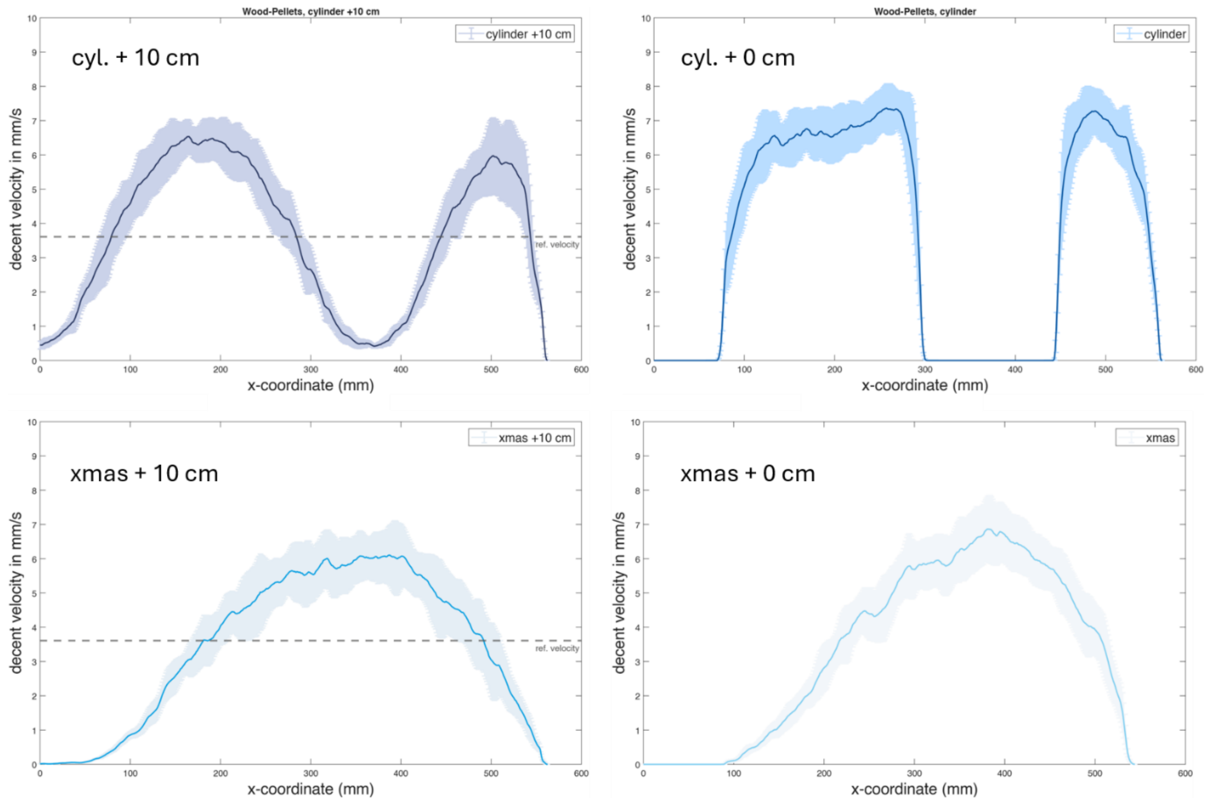

Figure 13: Sequence of decent velocity development and variance for wood spheres decending down the demonstration shaft shown for four defined evaluation levels

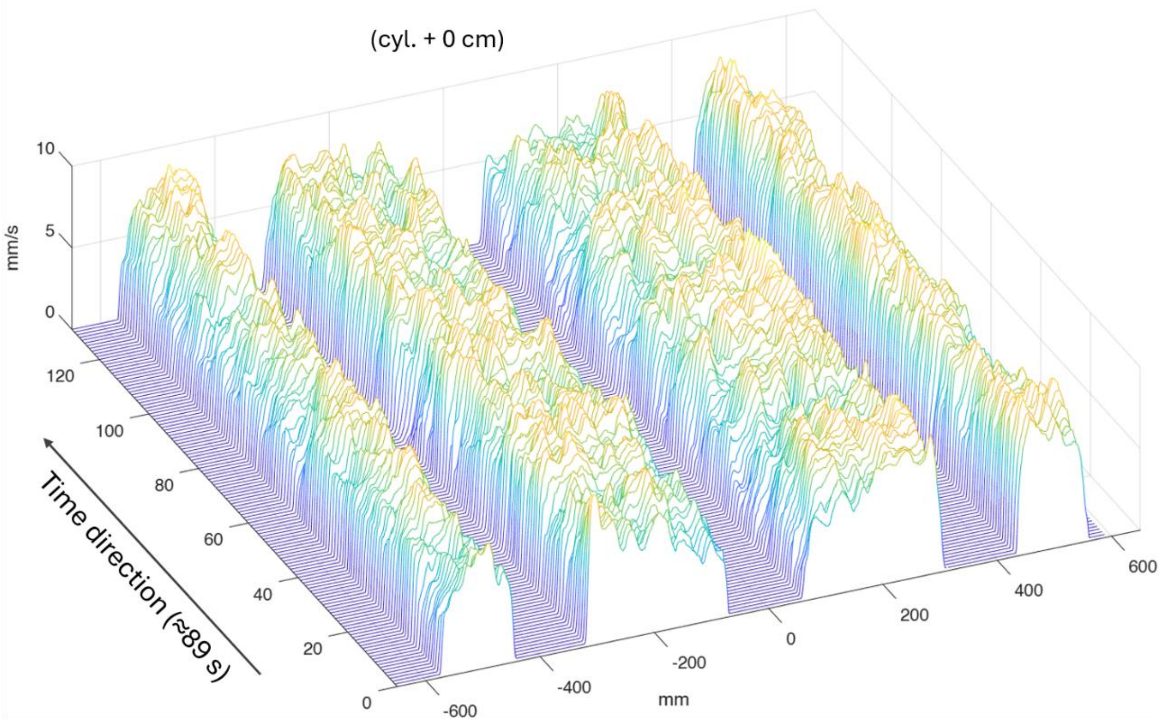

Figure 14: Velocity evaluation over time of experiment, each curve represents the decent velocity development over shaft construction width for 131 random sample over approx. 89 seconds on evaluation level “cylinder + 0 cm”.

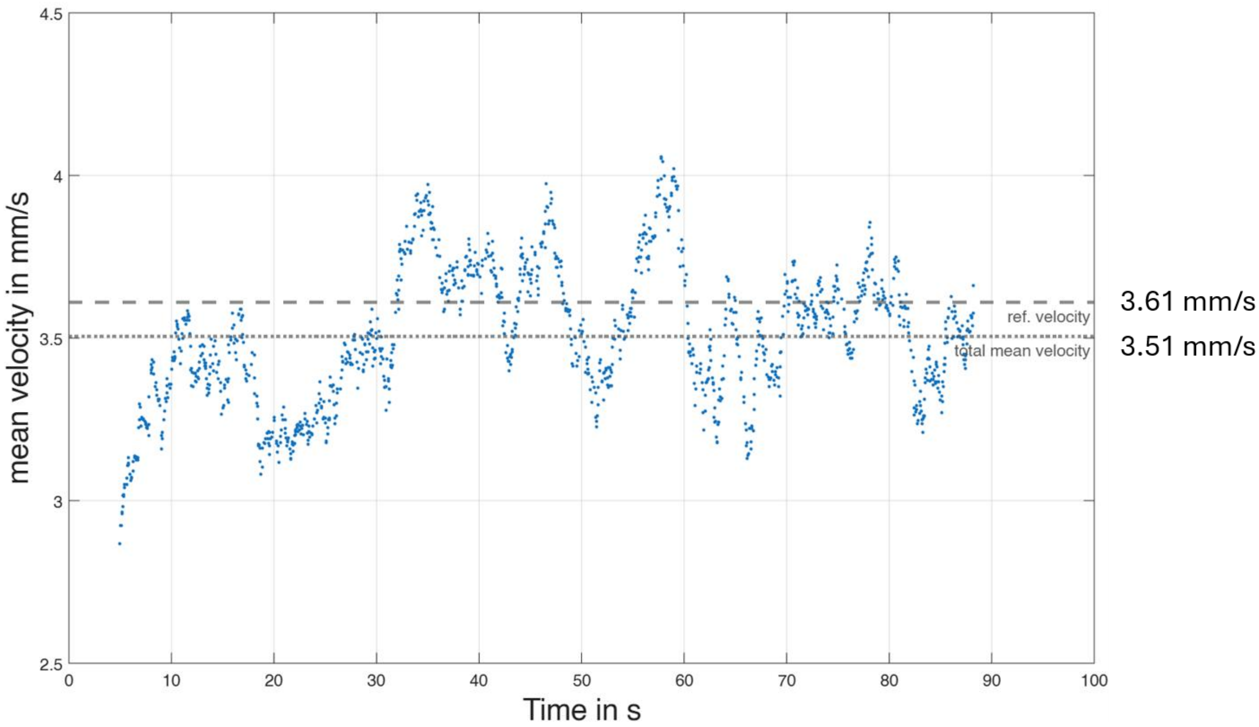

Figure 15: Mean decent velocity development over time of each accepted velocity matrix on level “cyl. + 10 cm”, total video length approx. 89 second

The curves shows the mean velocity over time on level 1 (Cyl. + 10 cm), derived from the matrices remaining after filtering. The temporal profile reveals that the decent velocity is lower at the beginning of the trial (till 1000 frames, ≈33 s) than in the remaining trial time and has a maximum in the middle part of the trial (over 4 mm/s). One possible explanation is that it takes time for the particle motion to build up at the beginning of the trail (transient part) until it reaches constant descent conditions. The total mean velocity deviates just about 0.1 mm/s from the reference decent velocity. This indicates a huge improve of data quality resulting from the new procedure as described above.

As last plausibility check to verify the application of the filter and the entire data processing method, the mass continuity of the determined descent velocities was checked by calculating the particle volume flow on each evaluation level. This volume flow should be generally consistent, though it is not expected to be completely constant due to the somewhat irregular decent of particle. This temporarily respectively locally leads to varying bulk voidage and to deviations of the local volume flow respectively mass continuity.

This final plausibility check was done basing on the corresponding mean velocity and is shown in Figure 16. The volume flow considers the different areas of the four defined evaluation levels. The reference volume flow of 1.22 dm^3/s, resulting from the measured surface decent velocity, is depicted as reference value in the plot in Figure 16. Only small deviations are recognisable for the first levels 1-3. The last level at the top of the “christmas tree” (level 4), shows the highest deviation. This may be a result of the filtering approach (removal of entire velocity matrices), local regions that exhibited higher or lower descent velocities—and which are not distorted—may have been removed because they were excluded based on the global filtering criteria. These local regions can then influence the locally calculated velocity (levels 1–4) derived from all remaining matrices. However, due to the strong change of the free flow cross-section at level 4 due to the large “christmas tree” installation, complete consistency of the balances cannot be expected in this area. Anyway, moderate inconsistencies within the overall balances are no issue for the calibration of the models, since the models themselves ensure closed balances.

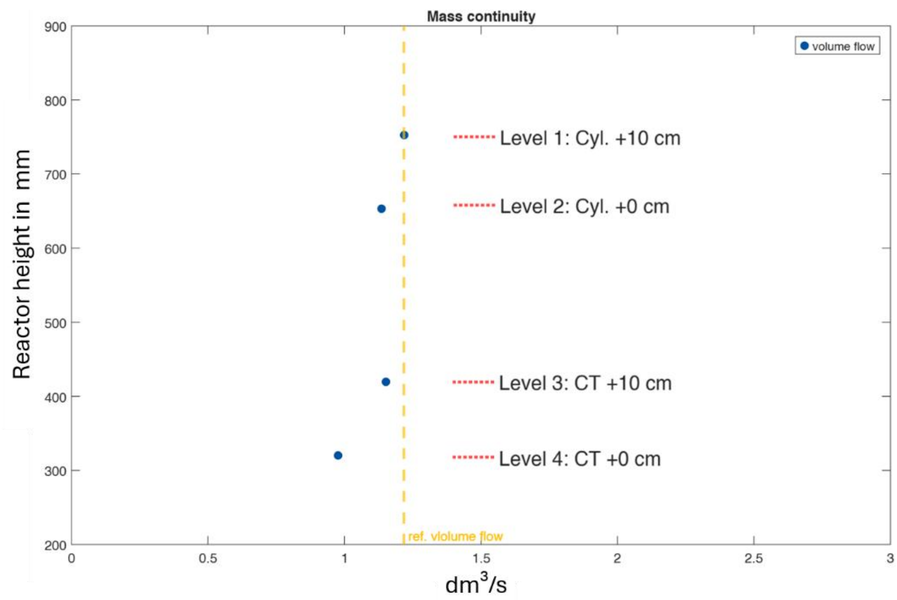

Figure 16 : Mass continuity of wood pellets evaluation, depicted as particle volume flow of wood pellets over shaft construction height for each evaluation level, reference volume flow: 1.22 dm^3/s, based on surface decent velocity.

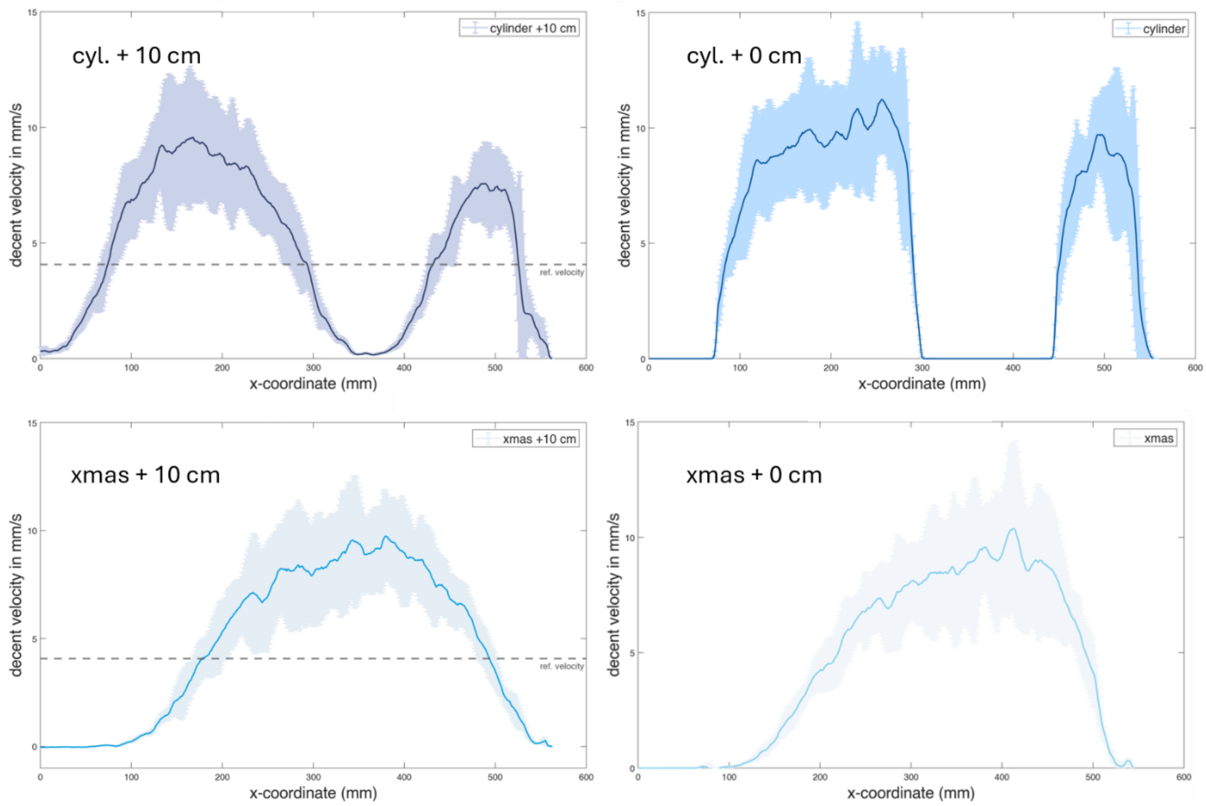

Figure 17: Sequence of decent velocity development and variance for clay particles, depicted for different evaluation levels.

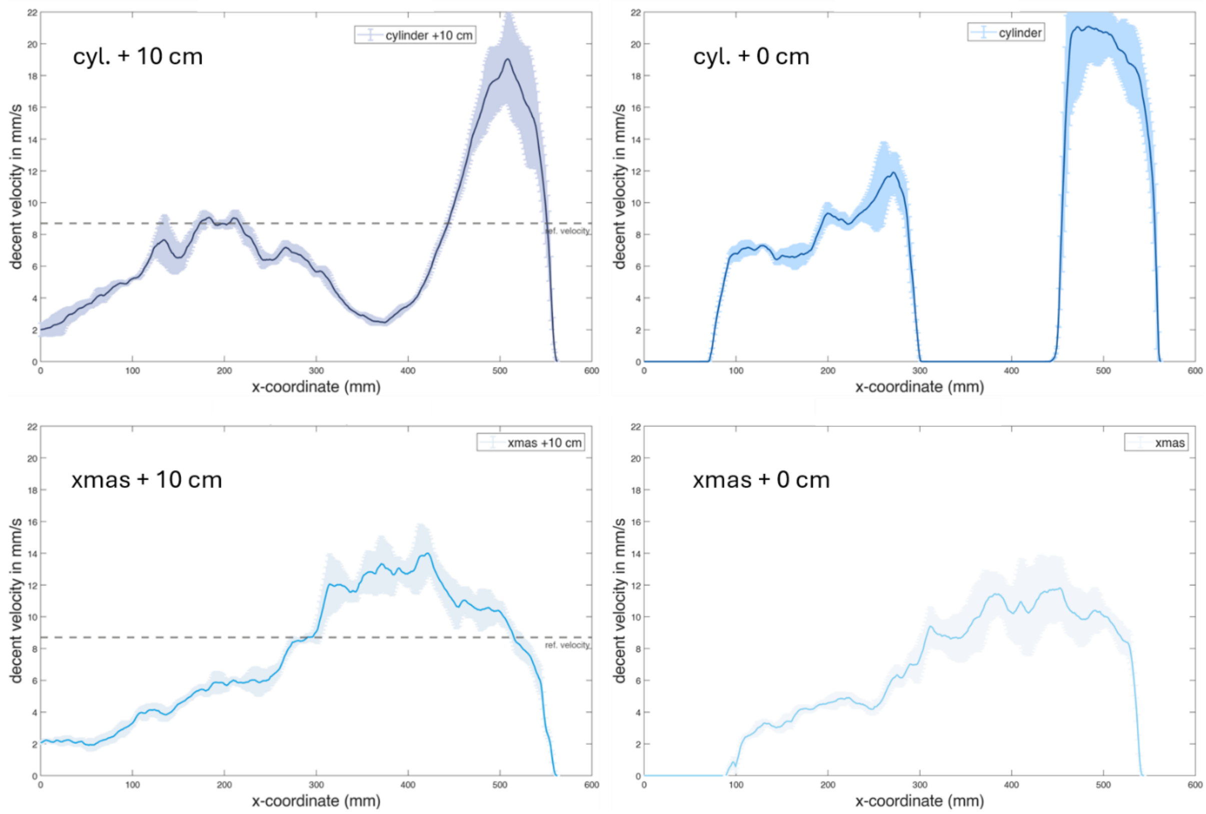

Figure 18: Sequence of decent velocity development and variance for DR-Pellets, depicted for different evaluation levels.

The determined velocity profiles for the remaining particle types (clay particle and DR-Pellets) on the defined evaluation levels, are shown in Figure 17 and Figure 18. The local velocity profiles were determined using the method explained above. However, depending on the camera orientation, the geometric boundary conditions and in dependence of the particle type and size, the threshold values for removing outliers must be adjusted for each experiment.

Figure 19 shows a comparison of the decent velocities at level 3 (CT + 10 cm) of all particle types. The results for DR pellets and clay pellets are exploited for the further evaluations, respectively the calibration of the DEM- and FEM-model. While the DR pellets results benefit from similar material properties compared to real industrial conditions, the clay pellets provide a more realistic ratio of particle size to demonstrator size.

Concluding, the new evaluation procedure shows a huge improvement of results for all considered particle types (DR, clay and wood pellets) despite the extremely difficult conditions impacting the optical evaluation like poor particle recognisability due to heterogeneous surface and low contrasts as well as reflections, vibrations, scratches and dust deposits on the window of the shaft construction apparatus. In consequence the new results enable a reliable model calibration.

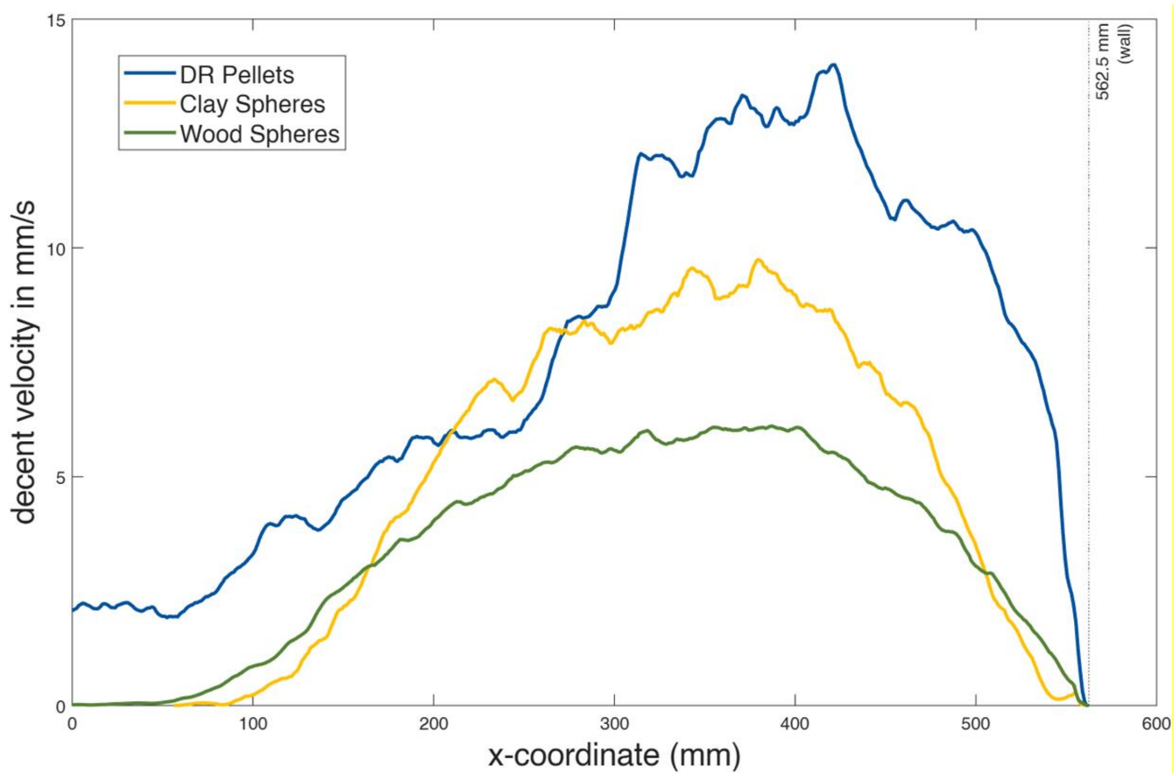

Figure 19: Comparison of decent velocities on level 3 (Cly. + 10 cm) from DR Pellets, clay- and wood spheres

3.3 DEM Simulations (RUB)

DEM simulations were carried out for the same conditions as the experiments to allow a direct comparison. Simulations were performed for both, DR-Pellets and clay pellets, without gas flow and with internal installations in place. A slide opening of 106 mm was used for the DR-Pellets and 52 mm for the clay pellets. Particle velocities were evaluated at the same measurement heights as in the experiments: 10 cm above the bolts and 10 cm above the "Christmas tree" installation.

Model calculations require the direct implementation of parameters such as tangential and normal spring stiffness. Rather than using direct calculations, mass-related model parameters were determined (Kruggel-Emden, Simsek, Rickelt, Wirtz, & Scherer, 2007)) ((Shäfer, Dippel, & Wolf, 1996)). As a result, input variables like the restitution coefficient, the tangential ratio to normal spring stiffness, and the contact time were necessary to apply the linear spring-dashpot model ((Shäfer, Dippel, & Wolf, 1996), (Kruggel-Emden, Wirtz, & Scherer, A study on tangential force laws applicable to he discrete element method (DEM) for materials with viscoelastic or plastic behavior, 2008).

Table 2: Interaction properties for contact between particles and particle-wall contact for DR-Pellets (a), wood spheres (b) and clay pellets (c).

Interaction parameters	***Particle – Particle***	***Particle – Walls***
μ (friction coefficient)	0.9	0.9
Collision time	1.0e-3	8.0e-4
e_n (restitution coefficient)	0.1	0.1
κ (stiffness parameter)	0.5	0.4
μ_r Rolling resistance (m)	0.15	4.0e-4

(a) DR-pellets

Interaction parameters	***Particle – Particle***	***Particle – Walls***
μ (friction coefficient)	0.6	0.6
Collision time	4.0e-3	6.0e-3
e_n (restitution coefficient)	0.45	0.5
κ (stiffness parameter)	0.3	0.4
μ_r Rolling resistance (m)	2.0e-1	3.0e-1

(b) wood spheres

Interaction parameters	***Particle – Particle***	***Particle – Walls***
μ (friction coefficient)	0.5	0.5
Collision time	3.0e-3	4.0e-3
e_n (restitution coefficient)	0.35	0.4
κ (stiffness parameter)	0.3	0.4
μ_r Rolling resistance (m)	1.2e-1	8.0e-2

(c) clay pellets

Because the DEM model currently uses spherical particles, it cannot capture the natural interlocking of an uneven or jagged surface. The sliding friction coefficient is therefore increased to reproduce the material's measured bulk behavior. The shaft furnace was filled with particles until a height of 2.3 meters from the base. To replicate this in the simulation, a total of 176,000 particles were generated.

To validate the DEM model, the simulated particle velocity distributions were compared with the experimental measurements obtained from particle tracking. The comparison was performed at two measurement locations inside the shaft: directly above the Christmas tree (CT) installation and 10 cm above the Christmas tree. These locations were selected because they represent regions where the internal geometry has a strong influence on the particle flow field.

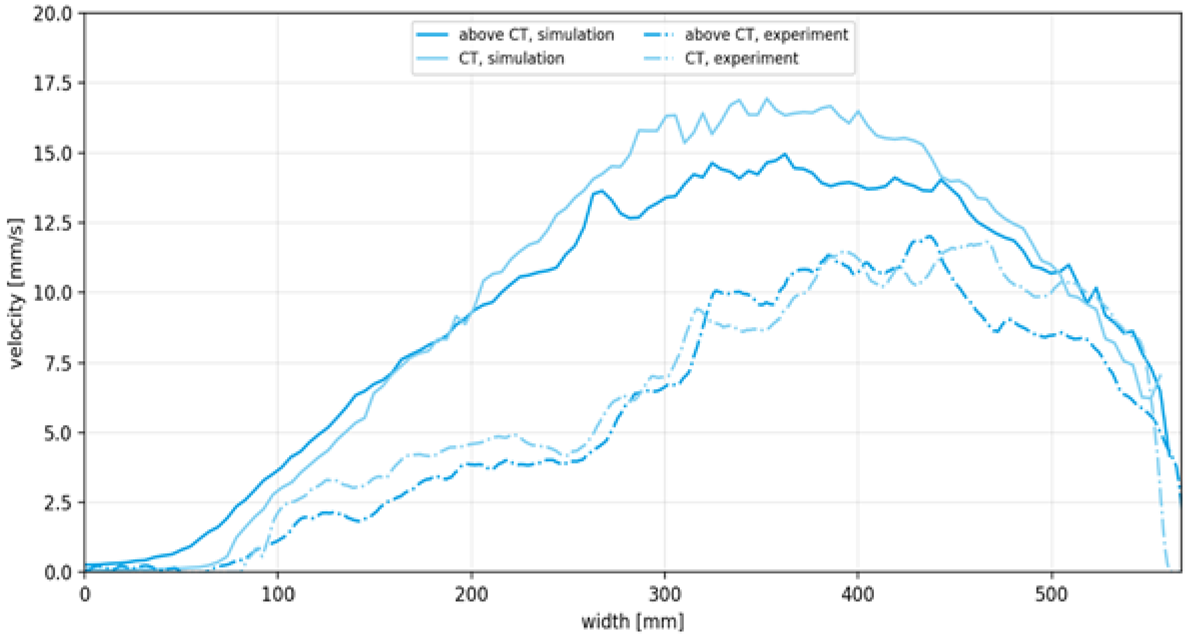

Figure 20: Comparison of DEM simulation and experimental particle velocity profiles for DR-Pellets at the CT level and 10 cm above the Christmas Tree (CT).

Figure 20 compares the velocity profiles obtained from the DEM simulations (solid lines) with the corresponding experimental measurements for DR pellets (dashed lines). Both datasets exhibit the same overall flow characteristics, with particle velocities increasing from the side walls towards the outlet region before decreasing again near the opposite wall. The simulations successfully reproduce the asymmetric influence of the internal installations and the location of the high-velocity regions.

With the parameter set of Table 2 the DEM model predicts overall higher particle velocities than those measured experimentally, especially around the maximum velocity region. At the CT level, the simulated peak reaches approximately 16–17 mm/s, whereas the experiments indicate peak values of about 11–12 mm/s. A similar trend is observed at the measurement location 10 cm above the Christmas tree, where the simulation predicts peak velocities around 14–15 mm/s, compared with approximately 11–12 mm/s in the experiments. These differences indicate that the predicted particle velocities are sensitive to the selected DEM parameters and can be adjusted by modifying the parameter values. Nevertheless, the numerical model captures the overall shape of the velocity distribution and correctly reproduces the influence of the internal geometry on the descending burden.

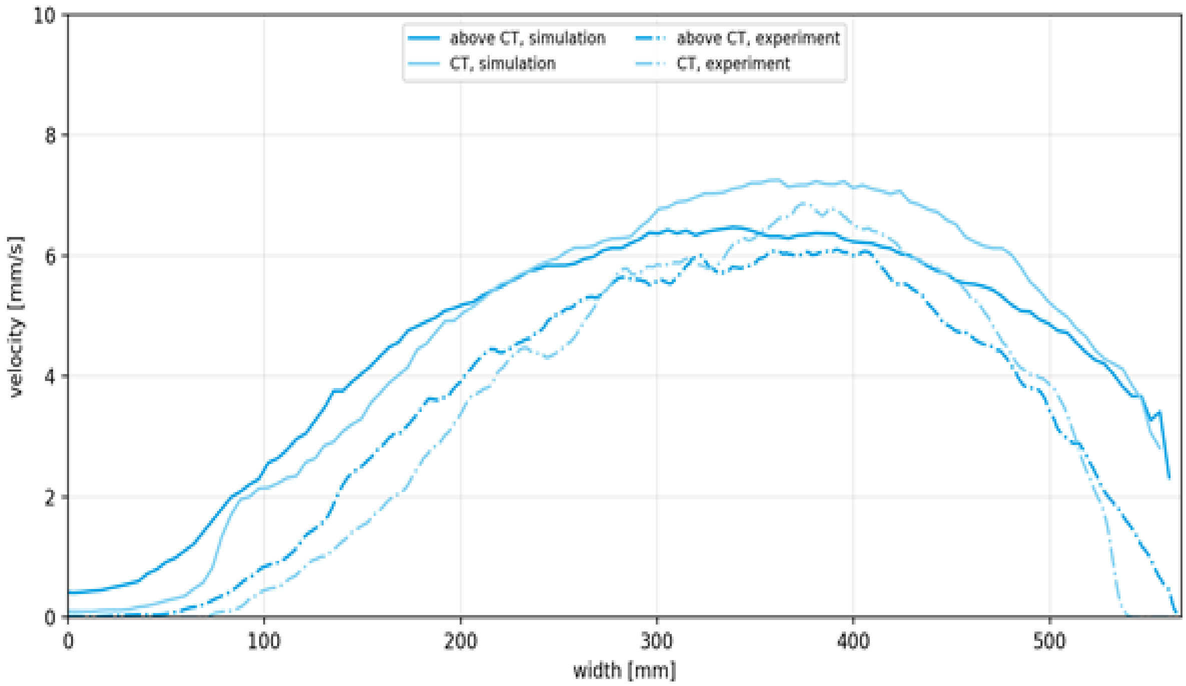

Figure 21: Comparison of DEM simulation and experimental particle velocity profiles for clay pellets at the CT level and 10 cm above the Christmas tree.

Figure 21 presents the comparison between DEM simulations (solid lines) and experiments (dashed lines) for the clay pellet material. As observed for the DR-Pellets, the simulations reproduce the general shape of the velocity profiles and the influence of internal installations on the particle flow. Particle velocities gradually increase towards the outlet region and decrease again close to the side walls. The agreement between simulation and experiment is better for the clay pellets than for the DR-Pellets. At both measurement locations, the simulated peak velocities differ from the experiments by less than approximately 1 mm/s over most of the profile.

A different approach was used for simulations with clay pellets. It should be noted that the DEM simulations shown were performed using 12 mm clay pellets, whereas the corresponding experiments were conducted with 6 mm clay pellets. This simplification was necessary because simulating the actual 6 mm particles would have required approximately ten times more particles, resulting in a computational effort that exceeded the available resources. All other material properties and contact parameters were kept identical to those of the experimental clay pellets, with only the particle diameter being modified. Consequently, the comparison between simulation and experiment should be interpreted with caution, as the difference in particle size influences the packing structure, contact network, porosity, and flow behavior. Although the simulations reproduce the overall velocity distribution and the main flow characteristics, quantitative deviations are expected due to this unavoidable scaling of the particle size.

Finally, Figure 22 presents the comparison between DEM simulations (solid lines) and experiments (dashed lines) for the wood spheres. The consistency is moderate with deviations towards center and wall. That may indicate that, the wall friction in the model should be higher.

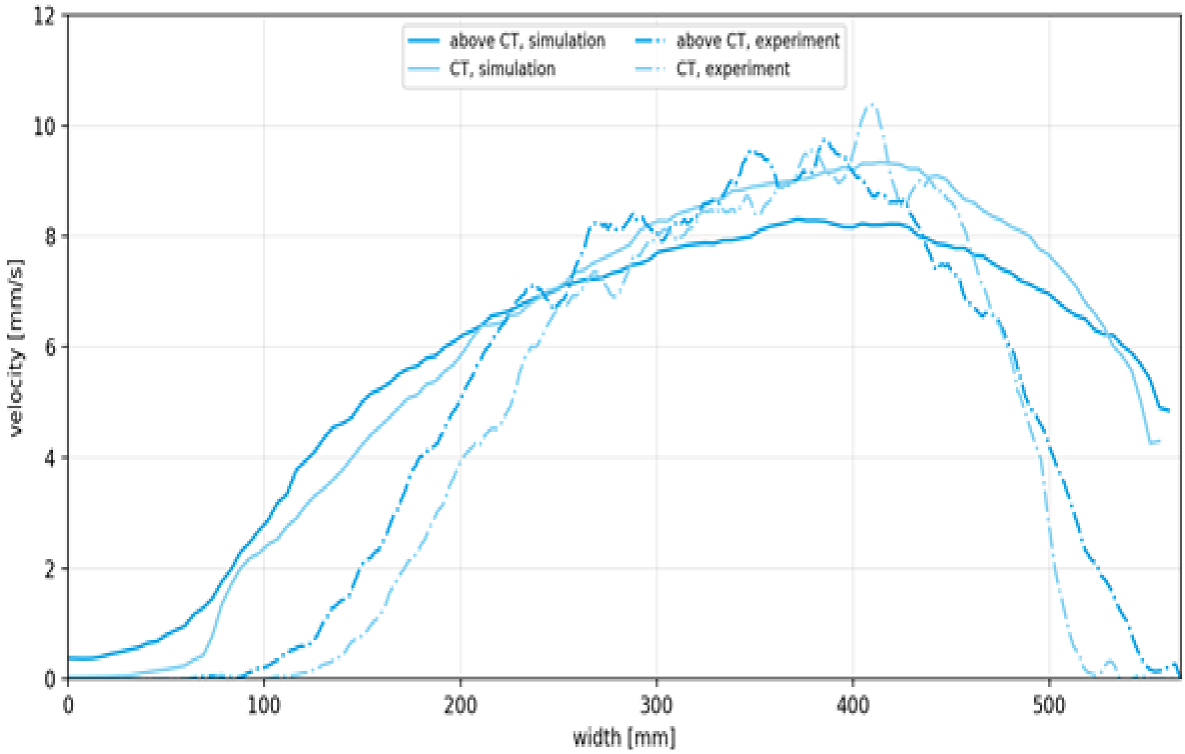

Figure 22: Comparison of DEM simulation and experimental particle velocity profiles for wood spheres at the CT level and 10 cm above the Christmas tree.

Overall, the comparison demonstrates that the DEM model accurately captures the dominant flow behavior for both materials under cold-flow conditions. The remaining differences mainly originate from uncertainties in the particle contact parameters and the simplified representation of real particle morphology. These validation results provide confidence in the numerical model and establish a reliable basis for the next set of coupled DEM-CFD simulations under gas-flow conditions.

3.4 Additional simulations RUB

The next set of simulations focuses on dynamic operating conditions, in which both, particle outflow and gas inflow are modeled simultaneously inside the MIDREX-based shaft furnace. In contrast to the previous cases, a gas stream of 1200 m^3/h is introduced through the inlets to reproduce the conditions of the corresponding experiments. This setup enables the coupled DEM-CFD model to capture the interaction between the descending burden and the upward-flowing gas under realistic, time-dependent conditions. The results from these dynamic simulations are then compared with the experimental measurements. Figure 23 below compares the pressure drop between experiments (bright) and simulations (dark).

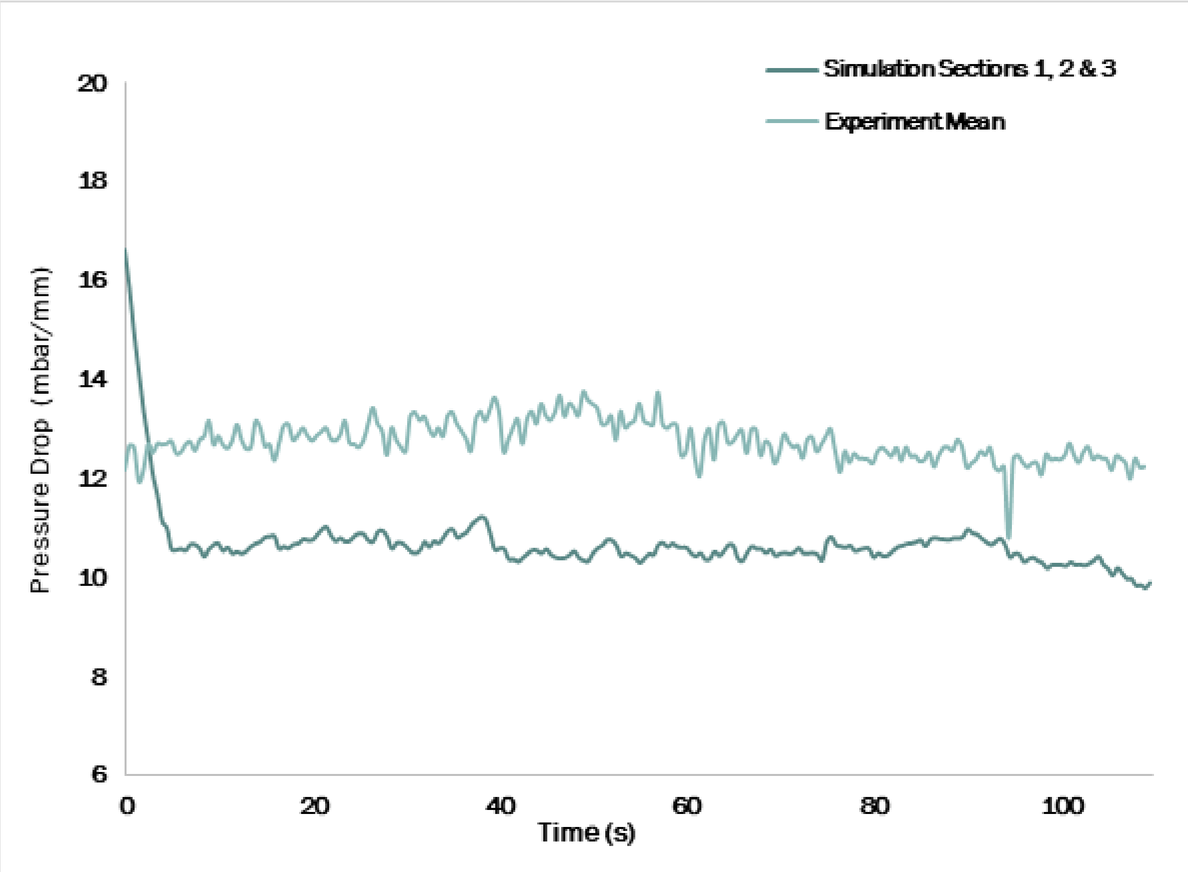

Figure 23: Comparison of outflow rate between all experiments and simulation

Figure 24 displays bulk and flow in the furnace during the simulation a time step 0, 40s, 80s, 120s. Initially, the bed is relatively uniform with low particle velocities and a homogeneous porosity distribution. As time progresses, particles accelerate downward, especially near the outlet, leading to bed compaction in the lower region and increased porosity variations. These changes influence the gas flow, which becomes more non-uniform, with higher velocities developing in regions of higher porosity and near the injection points.

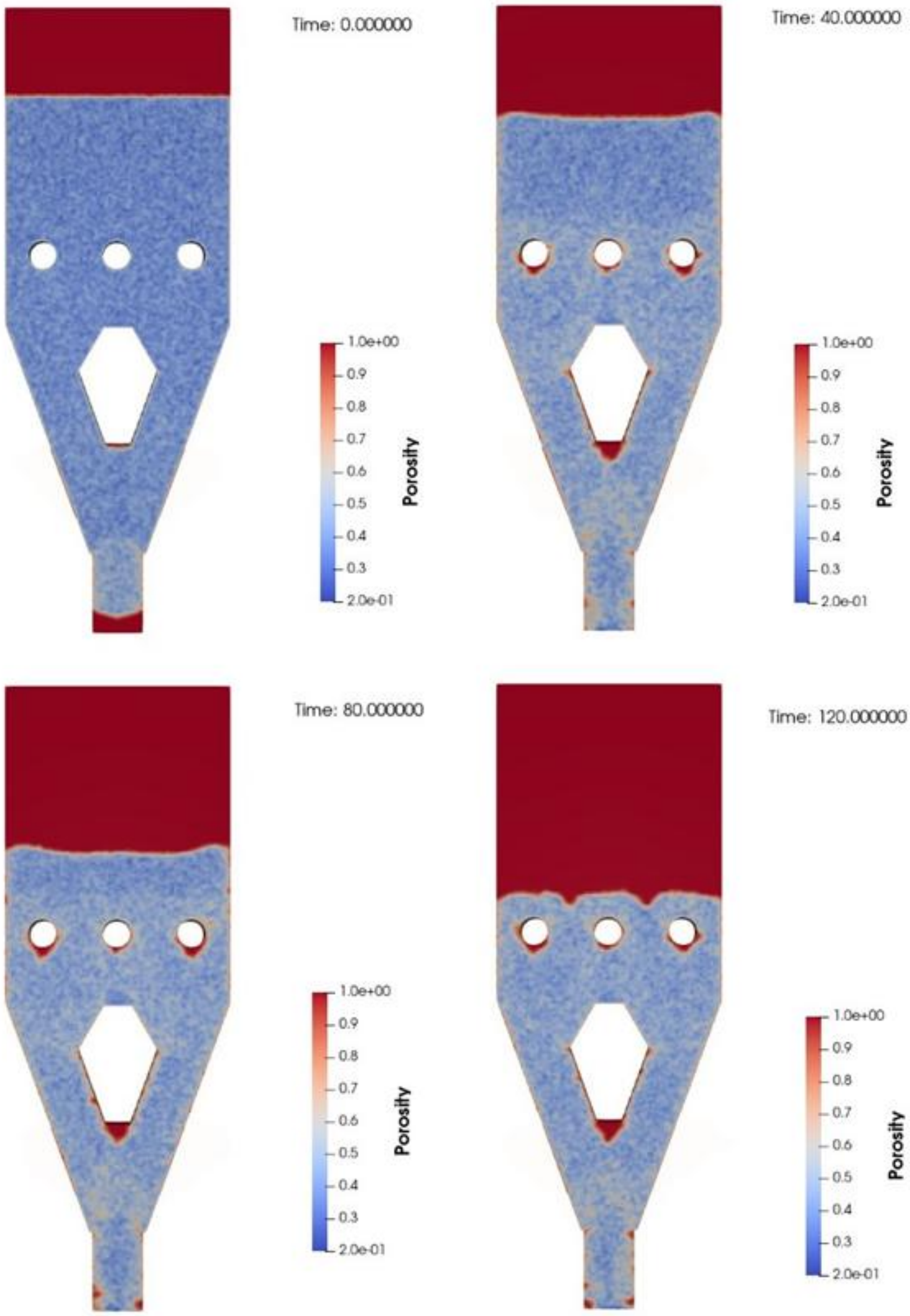
Time: 0.000000
Time: 40.000000
Time: 80.000000
Time: 120.000000
Porosity
1.0e+00
0.9
0.8
0.7
0.6
0.5
0.4
0.3
2.0e-01

(a)

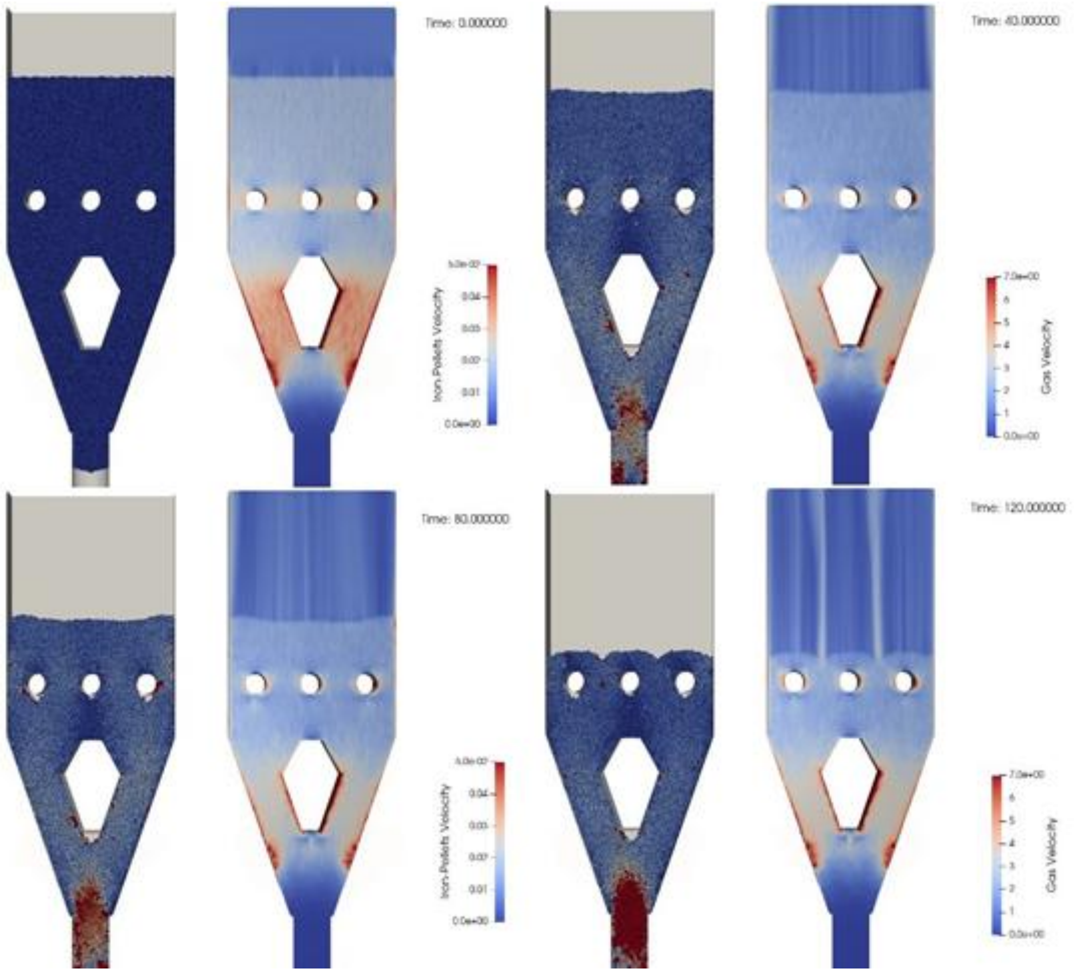

(b)

Figure 24: Particle porosity (a) and particle and fluid velocities (b) displayed in Paraview

3.5 Simulations FEM

Within the FEM code, the solid flow is represented by a rheology model (MaxH2DR, 2023) which enables an estimation of realistic solid descent profiles with very low computational effort, compared to the very expensive DEM simulation.

The general conditions are:

Wooden spheres	Clay pellets	DR-Pellets
Slide opening 60 mm	Slide opening 52 mm	Slide opening 106 mm
With installations	With installations	With installations
Without gas flow	Without gas flow	Without gas flow

Wooden spheres, clay pellets, and DR-Pellets descent without gas flow as estimated by the rheology model are compared to the experimental measurements to verify the approach. As reference, the particle velocities at cut lines 10 cm above the cylindrical installations and 10 cm above the Christmas tree are compared. In Figure 25 for DR pellets model results are shown as solid lines, experimental results as dashed lines. The following figures show the same results for clay pellets and wood spheres.

It can be concluded that the trends of solid decent profiles are generally consistent to the experimental results and large deviations just occur close to walls. This can be minimised by adjusting the wall friction settings of the rheology model. The approach can therefore be seen as validated as foreseen for the hybrid demonstration.

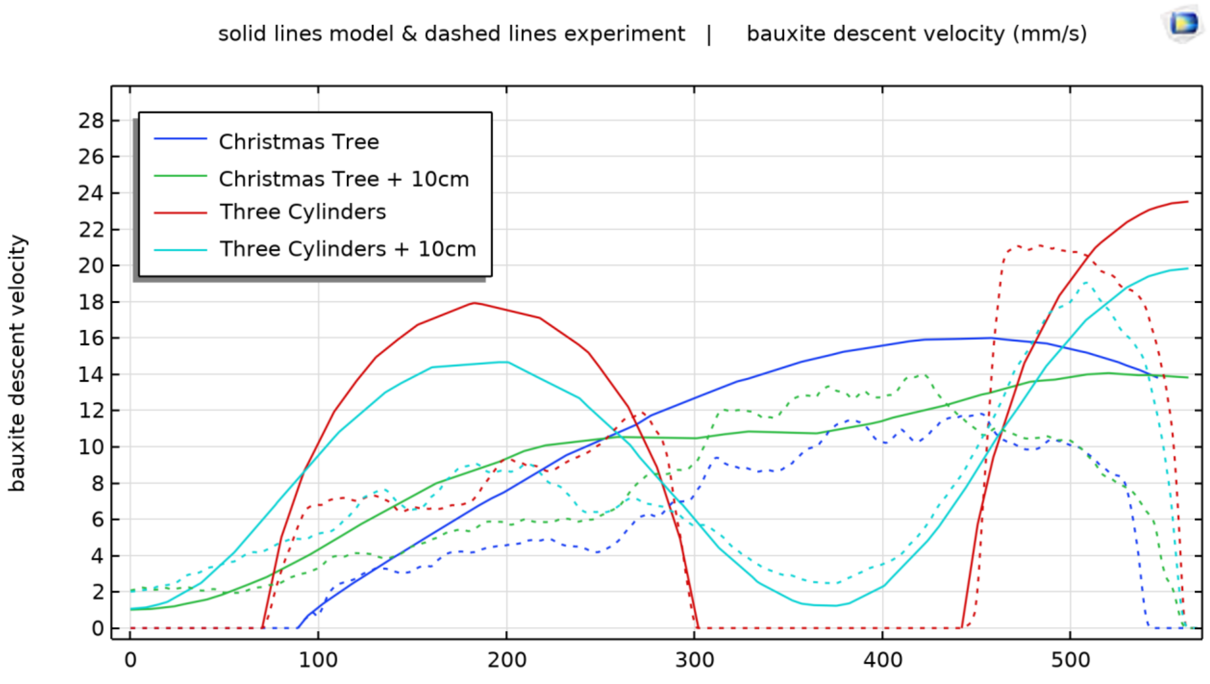

Figure 25: DR-Pellets descent experiment vs FEM Rheology model.

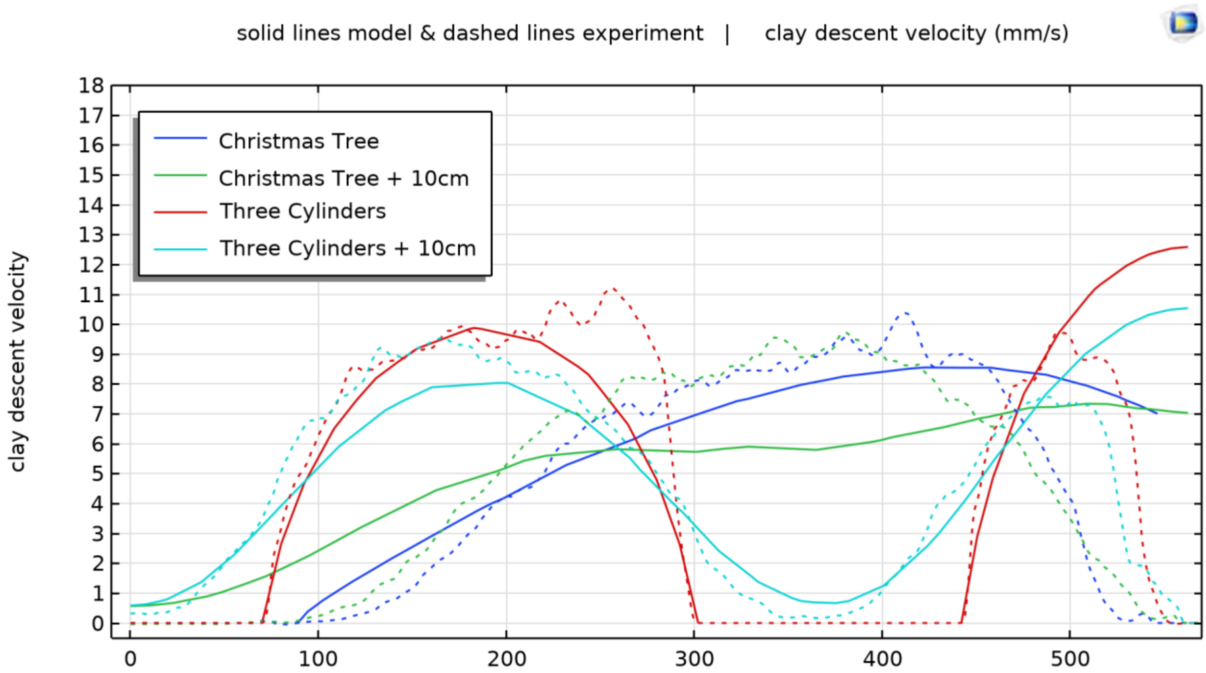

Figure 26: Clay pellets descent experiment vs FEM Rheology model.

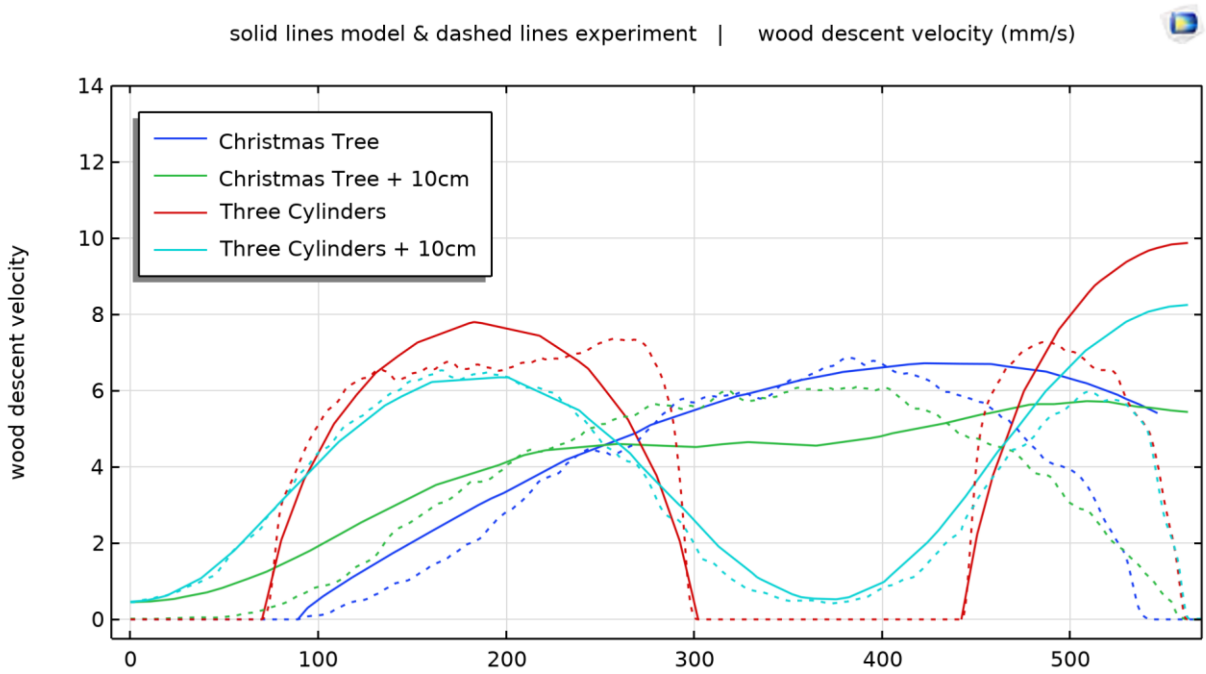

Figure 27: Wooden spheres descent experiment vs FEM Rheology model.

3.6 Comparison DEM and FEM

Figure 28 compares the different particle velocity profiles for DR-Pellets, as predicted for the Midrex based physical demonstrator by the DEM model developed at RUB (solid blue lines), by the rheology model developed at BFI (dashed blue lines), and as received by the experimental measurements (solid grey lines).

Both numerical models reproduce the general flow behaviour, showing increasing particle velocities from the side walls towards the outlet region followed by a gradual decrease near the middle of the furnace. Both models predict higher velocities than the experiments. This can be minimised by modifying the sensible particle outflow conditions. The rheology model produces smoother velocity profiles with a more gradual increase across the shaft width than the DEM model which seems reasonable considering the rheology approach which basically mimics solid flow like a kind of fluid. Close to walls the DEM model is consistent to the experimental results while the rheology model is clearly higher. This will be minimised in the next calibration steps.

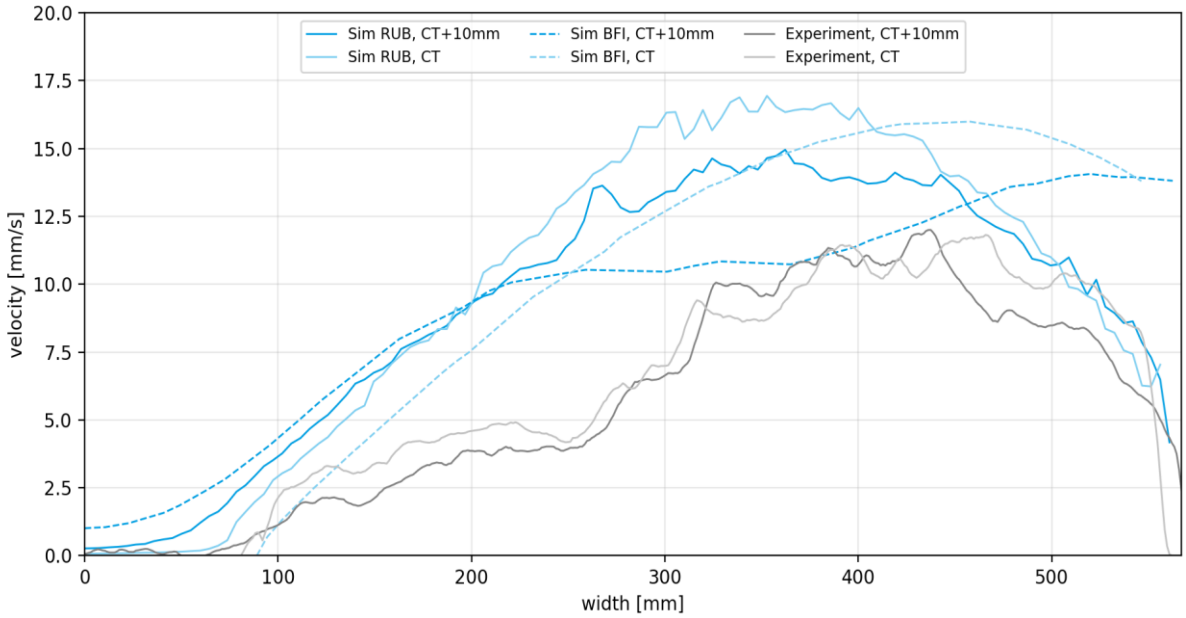

Figure 28: Comparison of particle velocity profiles for DR-Pellets obtained from the RUB model, the BFI model and the experiments.

Generally, the experimental results lie between the two numerical predictions over much of the domain, indicating that both models capture the dominant flow mechanisms but differ in the calibration of the particle contact behaviour. The remaining discrepancies are mainly observed in regions near to walls where high local velocity gradients exist and particle rearrangement and void formation have a stronger influence on the measured velocities. The discrepancies near the wall can be minimised by raising the model wall friction parameters for the final tuning.

Figure 30 compares the velocity profiles for clay pellets obtained from the RUB and BFI simulations with the experimental measurements. Both numerical models reproduce the overall shape of the measured velocity distribution and correctly identify the location of the maximum particle velocity above the outlet region. The RUB simulation shows very good agreement with the experiments over the central part of the shaft, although it slightly underestimates the peak velocity and predicts smoother transitions than those measured experimentally. In contrast, the BFI simulation produces a flatter velocity distribution and generally predicts higher velocities in the downstream region, resulting in larger deviations from the measurements. Despite these differences, both models successfully capture the influence of the internal installations on the particle flow. The comparison demonstrates that the two modelling approaches consistently reproduce the global flow pattern.

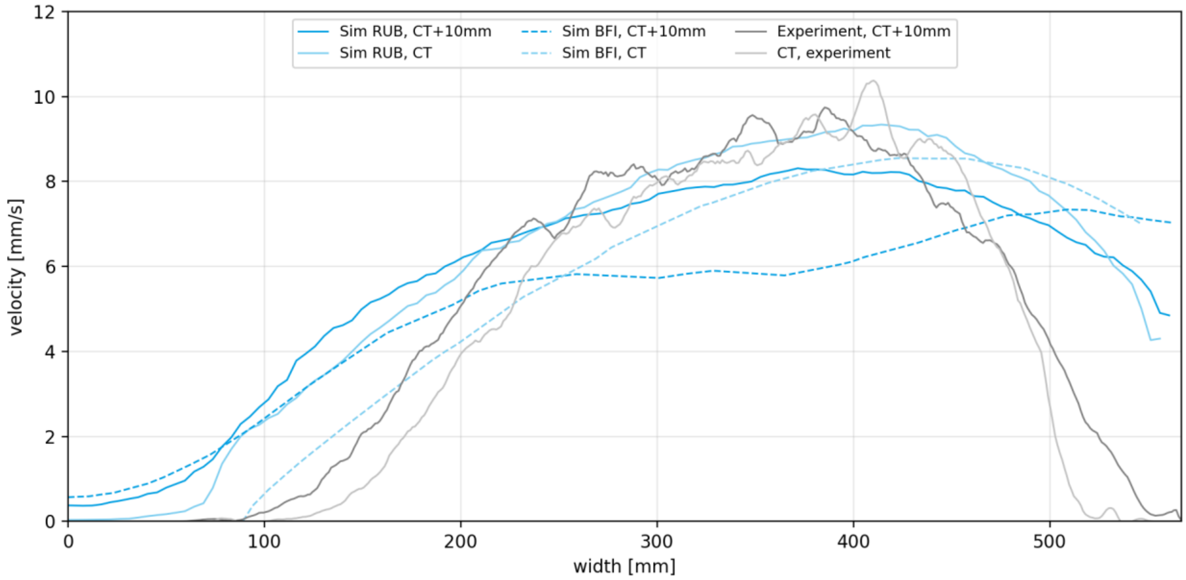

Figure 29: Comparison of particle velocity profiles for clay pellets obtained from the RUB model, the BFI model and the experiments.

Figure 30 presents the comparison for the wooden sphere experiments. The three datasets exhibit similar velocity distributions, with particle velocities increasing towards the central discharge region before decreasing near the side walls. The RUB simulation follows the experimental measurements closely over most of the shaft width and reproduces both the location and magnitude of the maximum particle velocity with good accuracy. Moderate deviations just occur near the wall.

The BFI simulation predicts a smoother profile and maintains slightly higher velocities in the downstream region, resulting in an overestimation near the wall of the shaft furnace. This needs further tuning of the wall friction parameters.

Overall, both numerical approaches successfully reproduce the characteristic flow behaviour, while the RUB model provides a closer quantitative agreement with the experimental observations for this material.

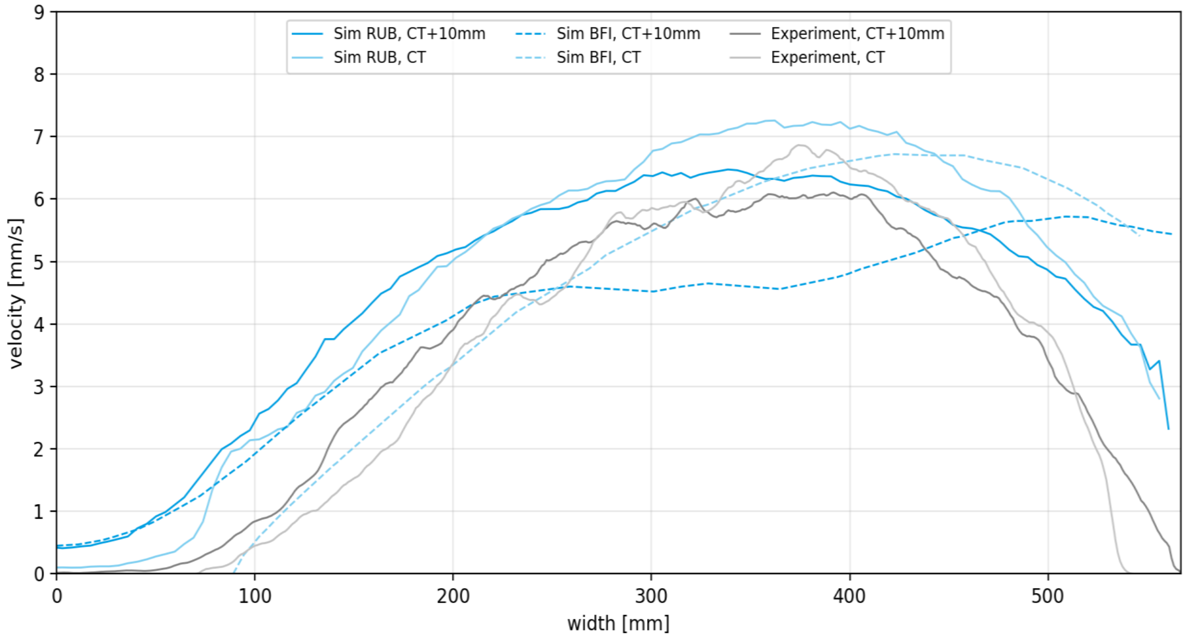

Figure 30: Comparison of particle velocity profiles for wood spheres obtained from the RUB model, the BFI model and the experiments.

Both the DEM model developed by RUB and the rheology model implemented by BFI successfully reproduced the main particle flow characteristics observed in the experiments. Some discrepancies exist close to walls which can be minimised by further parameter tuning.

While the DEM approach provides detailed particle-scale information, the continuum rheology model offers an efficient representation of the bulk material behaviour with very low computational effort. Overall, the agreement with the experimental measurements confirms that both modelling approaches are suitable for simulating solid flow in the demonstration-scale shaft furnace. Thus, they enable the hybrid demonstration as planned.

4. Summary and conclusions

This deliverable presented the experimental and numerical investigations needed to achieve the hybrid demonstration approach of MaxH2DR which fuses physical and digital investigations. Main focus was to determine the flow behaviour of granular materials in a demonstration-scale direct reduction shaft furnace representative of the MIDREX process. Experiments were conducted using DR-Pellets, wooden spheres, and clay pellets under cold-flow conditions without gas injection. Material properties, particle movement, and velocity distributions were measured to establish a dataset for validating numerical simulation models.

The particle-tracking code based on the PIV method was significantly improved to improve the reliability of the results. This substantially improved the data quality available for validating the DEM and FEM simulations.

DEM simulations were done using experimentally determined material properties and calibrated contact parameters to reproduce the observed bulk flow behaviour. The comparison between simulations and experiments demonstrated that the numerical model successfully captures the overall particle flow patterns, including the influence of the internal installations and the characteristic velocity distributions at different measurement heights. While some quantitative differences remain, particularly for the DR-Pellets where peak velocities are slightly overpredicted, the simulations reproduce the dominant flow mechanisms with a very good accuracy.

The FEM simulations were also validated against the experimental results, and benchmarked against the DEM results. For the wooden and clay spheres, the FEM results showed good agreement with the experimental data. For the DR-Pellets, however, clear discrepancies were observed close to the walls. The model parameters will be further adapted to improve the agreement between the simulations and the experimental results. The objective is to develop a robust model that provides reliable results for different materials with varying shapes, sizes, and densities.

Overall, the results presented in this deliverable describe the hybrid demonstration and validate that it provides a robust calibration of the further numerical modelling which will enable scale-up and process optimisation in the final tasks of MaxH2DR work package 2.

References

A. A. El-Geassy, V. R. (1985). Gaseous Reduction of Wustite with H2, CO and H2-CO Mixtures. *Transactions of the Iron and Steel Institute of Japan*, vol. 25, no. 6, p. 449-458.

Bohl, W. &. (2005). *Technische Strömungslehre.* Würzburg: Vogel Industrie Medien GmbH & Co. KG.

F. Patisson, D. A. (2000). Modeling of gas-solid reactions : kinetics, mass and heat transfer, and evolution of the pore structure. *Chemical Engineering and Technology*, vol. 23, no. 1, p. 75-79.

Geerdes, M., Chaigneau, R., Lingiardi, O., Molenaar, R., Van Opbergen, R., Sha, Y., & Warren, P. (2020). *Modern Blast Furnace Ironmaking.* Amsterdam: IOS Press.

Heikkilä, A., Iljana, M., Bartusch, H., & Fabritius, T. (2020). Reduction of iron ore pellets, sinter, and lump ore under simulated blast furnace conditions. *steel research international, 91*(11).

Hommel, J. e. (2018). Porosity–Permeability Relations for Evolving Pore Space: A Review with a Focus on (Bio-)geochemically Altered Porous Media. *Transp Porous Med. 124*.

Kitson, P., Mochón, J., Saxen, H., Böhnisch, S., Mernitx, J., & Hunger, J. (2003). *Optimisation of sinter plant operating conditions and BF burden material resources using advanced multivariate statistics.* Luxembourg City: Publications Office of the European Union.

Kraume, M. (2012). *Transportvorgänge in der Verfahrenstechnik.* Berlin: Springer.

Kruggel-Emden, H., Simsek, E., Rickelt, S., Wirtz, S., & Scherer, V. (2007). Review and extension of normal force models for the Discrete Element Method. *Powder Technol, vol. 171 no.3*, 157-173.

Kruggel-Emden, H., Wirtz, S., & Scherer, V. (2008). A study on tangential force laws applicable to he discrete element method (DEM) for materials with viscoelastic or plastic behavior. *Chemical Engineering Science, vol. 63, no. 6*, 1523-1541.

MaxH2DR. (2023). *Periodic report / Additional prefinancing report / Beneficiary termination report (HE): V1.1. European Commission, Horizon Europe, Grant Agreement No. 101058429.* European Commission.

Piontek, T., Hauck, T., Qyteti, K., Mahiques, E. I., & Scherer, V. (2026). *MaxH2DR, Deliverable 2.1 Physical demonstration of coupled solid and gas flow in DR shaft furnace.* European Commission.

Q. Fradet, M. K. (2023). Thermochemical reduction of iron oxide powders with hydrogen: Review of selected thermal analysis studies. *Thermochemica Acta*, vol. 726.

Qyteti, K., Piontek, T., Mahiques, E. I., Scherer, V., Kaymak, Y., Marx, K., & Hauck, T. (2024). *MaxH2DR, Deliverable 2.2 Digital demonstration of granular particle movement and fas flow by coupled DEM/CFD simulations.* European Commission.

Shäfer, J., Dippel, S., & Wolf, D. (1996). Force Schemes in Simulations of Granular Materials. *Journal de Physique I, vol. 6, no. 1*, 5-20.